Molecules **2013**, *18*, 11904-11937; doi:10.3390/molecules181011904

OPEN ACCESS

molecules

ISSN 1420-3049

www.mdpi.com/journal/molecules

Review

Measuring Dynamic and Kinetic Information in the Previously Inaccessible Supra-τ_c Window of Nanoseconds to Microseconds by Solution NMR Spectroscopy

David Ban [†], T. Michael Sabo [†], Christian Griesinger and Donghan Lee *

Department for NMR-based Structural Biology, Max-Planck Institute for Biophysical Chemistry, Am Fassberg 11, D-37077 Göttingen, Germany

[†] These authors contributed equally to this work.

* Author to whom correspondence should be addressed; E-Mail: dole@nmr.mpibpc.mpg.de; Tel.: +49-551-201-2251; Fax: +49-551-201-2202.

Received: 16 July 2013; in revised form: 28 August 2013 / Accepted: 17 September 2013 / Published: 26 September 2013

Abstract: Nuclear Magnetic Resonance (NMR) spectroscopy is a powerful tool that has enabled experimentalists to characterize molecular dynamics and kinetics spanning a wide range of time-scales from picoseconds to days. This review focuses on addressing the previously inaccessible supra-τ_c window (defined as τ_c < supra-τ_c < 40 μs; in which τ_c is the overall tumbling time of a molecule) from the perspective of local inter-nuclear vector dynamics extracted from residual dipolar couplings (RDCs) and from the perspective of conformational exchange captured by relaxation dispersion measurements (RD). The goal of the first section is to present a detailed analysis of how to extract protein dynamics encoded in RDCs and how to relate this information to protein functionality within the previously inaccessible supra-τ_c window. In the second section, the current state of the art for RD is analyzed, as well as the considerable progress toward pushing the sensitivity of RD further into the supra-τ_c scale by up to a factor of two (motion up to 25 μs). From the data obtained with these techniques and methodology, the importance of the supra-τ_c scale for protein function and molecular recognition is becoming increasingly clearer as the connection between motion on the supra-τ_c scale and protein functionality from the experimental side is further strengthened with results from molecular dynamics simulations.

Keywords: supra-τ_c; RDC; relaxation dispersion; $R_{1\rho}$; CPMG; protein dynamics; NMR spectroscopy

1. Introduction

One of the essential keystones for the existence of life rests in the intricate relationship between biomolecular function and structural dynamics. The biomolecular machines engaging in these indispensable processes possess internal structural dynamics on a wide range of time-scales. It is the relationship or connection between the time-scales of these fundamental biophysical phenomena and the time-scales of biomolecular dynamics that the technique of Nuclear Magnetic Resonance (NMR) spectroscopy is uniquely equipped to explore. NMR is a powerful technique whose observables are time-scale sensitive [1]. Given that the sample is tractable for NMR studies, the system can be explored in solution without chemical modification while maintaining atomic resolution.

A wide range of NMR experiments have been developed that report on a broad range of time-scales from picoseconds to more than seconds (Figure 1). Exchange Spectroscopy (Figure 1; EXSY) first demonstrated by Meier *et al.* in 1979 [2] is a NMR technique for investigating slow time-scale dynamics (~50 ms to more than seconds provided that the exchange process is not much slower than the longitudinal relaxation rate). Specifically slow processes can therefore be studied by EXSY on states of the density matrix with long longitudinal relaxation times [2]. EXSY was later applied to measure aromatic ring flips in BPTI [3], to monitor enzyme catalysis [4–6] and to follow folding processes [7,8]. NMR can also be implemented for the investigation of biophysical processes occurring so slowly that several free induction decays (FIDs) or even multidimensional spectra can be recorded while the system is pseudo-static. This type of experiment is called real-time NMR and utilizes the repetitious collection of NMR spectra. Real-time NMR has been applied to systems engaged in slow substrate turn-over events [9] and in folding processes [10]. Fast acquisition techniques [11–13] and hyperpolarization [14,15] have recently been invented with the goal of measuring faster kinetics as well as improving signal to noise. Additionally, the probed system adopts a range of distinctive structural configurations that may translate into differences in the NMR chemical shift. Depending on the time-scale for the structural changes, the chemical shift itself can also be used as a dynamic metric [16–19]. Chemical shifts have been predicted and used to report on sampled conformational sub-states from a recent 1 millisecond molecular dynamics (MD) trajectory of bovine pancreatic trypsin inhibitor (BPTI) [19,20]. Another important NMR parameter is the cross-correlated relaxation rate, which encapsulates the correlated nature of potentially synchronous inter-nuclear vector motion on time-scales spanning picoseconds to milliseconds [21–25].

In this review, we address the considerable progress that has been made to characterize the amplitude and time-scale of inter-nuclear vector dynamics within a window that remained as a "blind-spot" for NMR. This window covers about four orders of magnitude and ranges between the overall tumbling time of a molecule (τ_c) to 40 μs (Figure 1), but as we will see has been extended to ~25 μs [26] (Section 3). This previously inaccessible time window has been defined as the supra-τ_c range [27,28]. The use of experiments that report on motions faster than τ_c will also be mentioned as

well as the experiments denoted in Figure 1 as rotating frame longitudinal relaxation ($R_{1\rho}$) and Carr-Purcell-Meiboom-Gill (CPMG) experiments, which rely on the characterization of conformational exchange. The extraction of dynamical content from residual dipolar couplings (RDCs) and the measuring of kinetics from conformational exchange has implications for understanding the mechanisms of molecular recognition and protein function within the supra-τ_c scale.

Figure 1. The accessible time-scale for NMR observables and the respective limits for some NMR experiments.

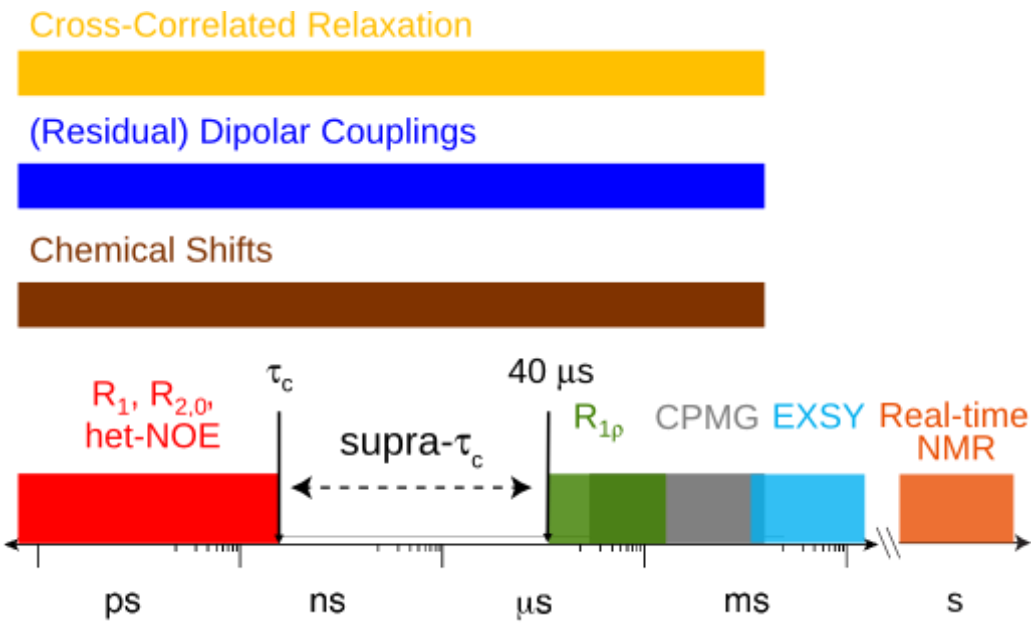

2. Dynamic Content of the Supra-τ_c Range

2.1. Introduction to Residual Dipolar Couplings

An essential NMR parameter that provides both structural and dynamic information including the supra-τ_c scale is the residual dipolar coupling (RDC) between two nuclear magnetic moments [29,30]. The beginnings of the RDC field can be traced back to 1963 when Saupe and Englert aligned benzene with *p*-azoxyanisole [31]. From here, the theoretical background for the analysis of RDCs for the extraction of structural and dynamic parameters has a rich history of development. Though this review does not aim to provide a detailed account concerning the history of the RDC field, nevertheless, we refer the reader to a comprehensive, yet not exhaustive, list of the pioneering work from Saupe [32,33], Snyder [34], MacLean and co-workers [35–37], Emsley and co-workers [38–44], and Pines and co-workers [45,46] toward the advancement of the theoretical underpinnings regarding solute alignment under anisotropic conditions.

In respect to biomolecules, thirty-two years passed from the initial report from Saupe and Englert [17] until Tolman and coworkers reported the first investigation of aligning cyanometmyoglobin, which possesses a paramagnetic center, in a magnetic field [47]. At the same time, Bolton and co-workers aligned a dodecamer of DNA in a magnetic field due to magnetic susceptibility of the unlabeled DNA [48]. A year later, Bax and colleagues described RDCs for the diamagnetic protein ubiquitin taken from

changes in N-H^N splitting resulting from varying magnetic susceptibility anisotropy at different static field strengths [49]. These couplings were quite small, on the order of 0.2 Hz, and an alternative method for measuring RDCs was proposed where the protein is dissolved in a partially anisotropic environment, the first being bicelles [9]. Since then, a multitude of alignment media have been described in the literature, including but not limited to filamentous phages [50–52], a mixture of cetylpyridinium bromide/chloride hexanol [53,54], a mixture of alkyl poly(ethylene glycol) and hexanol [55], a stretched [56,57] or a compressed polyacrylamide gel [58], and purple membrane fragments [59,60]. The advantage of these types of alignment media is that the strength of alignment is more under the experimentalist's control, producing RDC values several orders of magnitude higher than in the case of magnetic susceptibility anisotropy. For more information on the specifics of the different types of alignment media that are currently available, the reader is referred to the following reviews [61–63].

In the anisotropic media, all possible orientations for an inter-nuclear vector are populated with unequal probability, resulting in the dipolar couplings (*D*) no longer averaging to zero, with values on the order of 1/1000 the value of the maximal dipolar coupling. From an experimental standpoint, the RDC adds together with *J*-coupling, requiring two measurements to extract the RDCs: one in isotropic conditions to determine the *J*-coupling and one in anisotropic conditions to determine the (*J* + *D*)-coupling. Reviewed in several places, schemes for measuring the RDCs either rely on measuring the peak splitting in a coupled HSQC or the (*J* + *D*)- or *J*- coupling modulated peak intensity [61,64–66].

The main focus of this section is two-fold. First, a theoretical framework for utilizing RDCs in the determination of structural and dynamic properties for inter-nuclear vectors is described in detail. The measured RDCs encode a unique signature of the extent of supra-τ_c motion and methodology has been developed toward extracting this information in a robust manner. The second half of this section concentrates on some of the effort that has been invested in linking these amplitudes of supra-τ_c motion to biophysical phenomena, specifically molecular recognition. In particular, long MD trajectories, accelerated molecular dynamics simulations, and RDC restrained molecular dynamics simulations provide a more global picture of how these experimentally derived local dynamics could be relevant for function and stability.

2.2. Alignment Tensor Determination

Partial alignment of a protein results in the observed resonance splitting (Hz) for two nuclear spins to possess a contribution from the secular part of the magnetic dipole interaction:

$$D_k^{exp} = D_{ij}^{max}\langle(3\cos^2\theta_k - 1)/2\rangle \tag{1}$$

$$D_{ij}^{max} = -\frac{\mu_0\gamma_i\gamma_j\hbar}{4\pi^2 r_{ij}^3} \tag{2}$$

where μ_0 is the permeability of vacuum, γ_i and γ_j are the gyromagnetic ratios of nuclei *i* and *j*, $\hbar$ is Planck's constant, r_{ij} is the distance between nuclei *i* and *j*, and θ_k is the angle between the inter-nuclear vector formed by nuclear spin pair *k* and the magnetic field (B_0). The important concept to note from Equation (1) is that the magnitude of D_k^{exp} depends on $\langle(3\cos^2\theta_k - 1)/2\rangle$, which is ensemble averaged over the time-scale covered by the RDC measurement (denoted by the angular brackets). The

time-averaged or ensemble averaged information covers up to the millisecond time-scale or roughly $1/D$, spanning the supra-τ_c scale [30].

We will first consider the simplest case, theoretical analysis of a rigid molecule. In the absence of inter-nuclear vector dynamics, the instantaneous orientation of B_0 relative to each inter-nuclear vector within a protein or molecule can be defined in the molecular frame (MF), which is an arbitrary frame of reference usually given by the PDB coordinates. Each inter-nuclear vector can be defined by three angles, β_x, β_y, and β_z, between the vector and the respective MF axes. In a similar fashion, the vector parallel to B_0 can be expressed by three angles representing the instantaneous orientation of B_0 relative to the MF axes, α_x, α_y, and α_z. Within the MF, Equation (1) can be expressed as:

$$D_k^{exp} = D_{ij}^{max} B \cdot \langle A \rangle \tag{3}$$

where $B \cdot \langle A \rangle$ is the scalar product of two vectors representing the inter-nuclear orientations (B) and the B_0 orientations ($\langle A \rangle$). Both $\langle A \rangle$ and B contain 5 independent terms and are related to a 3 × 3 second rank Cartesian order tensor as follows [32–34]

$$\langle A \rangle = \left[a_{zz}, \frac{1}{\sqrt{3}}\left(a_{xx} - a_{yy}\right), \frac{2}{\sqrt{3}} a_{xz}, \frac{2}{\sqrt{3}} a_{yz}, \frac{2}{\sqrt{3}} a_{xy} \right]_l \tag{4}$$

where the averaged orientation of B_0 in the MF is given by:

$$a_{mn} = \langle \frac{1}{2} (3\cos\alpha_m \cos\alpha_n - \delta_{mn}) \rangle_l \tag{5}$$

and:

$$B = \left[b_{zz}^k, \frac{1}{\sqrt{3}}\left(b_{xx}^k - b_{yy}^k\right), \frac{2}{\sqrt{3}} b_{xz}^k, \frac{2}{\sqrt{3}} b_{yz}^k, \frac{2}{\sqrt{3}} b_{xy}^k \right] \tag{6}$$

where the orientation of the inter-nuclear vector in the MF is described by:

$$b_{mn}^k = \frac{1}{2} (3\cos\beta_m^k \cos\beta_n^k - \delta_{mn}) \tag{7}$$

The term δ_{mn} represents the Kronecker delta function, l is the alignment condition, and $m,n = x, y, z$. When a set of RDCs have been measured for a protein and the structural coordinates of the protein are known from a crystal or NMR structure, then Singular Value Decomposition (SVD) is typically used to calculate an exact solution for the alignment tensor, $\langle A \rangle$ [67]. Here, SVD of B is performed in order to obtain the pseudo-inverse of B, B^+. With B^+, the following equation determines $\langle A \rangle$ through left multiplication of Equation (3) with B^+:

$$\langle A \rangle = B^+ \frac{D_k^{exp}}{D_{ij}^{max}}. \tag{8}$$

The SVD approach requires that the RDC measurement includes at least five inter-nuclear vectors sampling at least five independent orientations, leading to a nonsingular B matrix and thus $B^+B = 1$, or the identity matrix.

The calculated alignment tensor can be recast into a symmetric 3 x 3 second rank Cartesian order tensor, $\left(\langle A^{(2)} \rangle\right)$ and then redefined in a principal axis system (PAS), termed the alignment frame (AF), where Equation (1) becomes [61]:

$$D_{k,l}^{exp} = D_a \left[3\cos^2\theta_k^{AF} - 1 + \frac{3}{2} R(\sin^2\theta_k^{AF}\cos 2\phi_k^{AF}) \right] \tag{9}$$

In Equation (9), the magnitude of the alignment tensor is $D_a = \frac{1}{2} D_{ij}^{max} * A_{zz}^{PAS}$, the rhombicity is $R = \frac{2(A_{xx}^{PAS} - A_{yy}^{PAS})}{3 * A_{zz}^{PAS}}$, $(\theta_k^{AF}, \phi_k^{AF})$ are the polar angles defining the inter-nuclear vector in the AF, and A_{mm}^{PAS} are the eigenvalues resulting from the diagonalization of $\langle A^{(2)} \rangle$. From the eigenvectors (A_{mn}^{EV}), the Euler angles describing the rotation of $\langle A \rangle$ and B into the PAS are defined:

$$\alpha = \arctan\left[A_{xz}^{EV}, A_{yz}^{EV}\right], \beta = \arccos[A_{zz}^{EV}], \gamma = \arctan\left[-A_{zx}^{EV}, A_{zy}^{EV}\right]. \tag{10}$$

In the case where multiple RDC sets are available for a given biomolecule, Joel Tolman developed a compact matrix formalism to calculate alignment tensor information in a more intuitive manner [68]. When *K* RDCs are measured under *L* alignments, then Equation (3) becomes:

$$\mathbf{D} = \mathbf{B}\langle \mathbf{A} \rangle \tag{11}$$

where **D** is a *K* x *L* matrix, **B** is a *K* x 5 matrix, and $\langle \mathbf{A} \rangle$ is a 5 x *L* matrix. In Equation (11), the term D_{ij}^{max} is included in $\langle \mathbf{A} \rangle$. The rows of **B** are defined by Equation (6) and the columns of **A** are given by Equation (4). As with the SVD approach to a single alignment media, the calculation of $\langle \mathbf{A} \rangle$ for all alignment media at once requires a nonsingular **B** matrix:

$$\langle \mathbf{A} \rangle = \mathbf{B}^{+}\mathbf{D} \tag{12}$$

where $\mathbf{B}^{+}$ is the pseudo-inverse of **B**. As mentioned above, each alignment tensor can be rotated into a PAS and the five parameters describing the alignment, $\{D_a, R, \alpha, \beta, \gamma\}_l$, can be extracted with Equations (9) and (10). It should be mentioned that several programs exist for the calculation of alignment tensor information, such as PALES [69,70] and REDCAT [71].

2.3. Model Free Analysis and Direct Interpretation of Dipolar Couplings

In reality, the molecules under investigation are not static and ensemble averaging of the RDC observable must also be considered. To calculate the dynamical content from the RDC data, five orthogonal alignment media must be measured for the system under investigation. This requirement is in analogy to the determination of an alignment tensor, where at least five orthogonal inter-nuclear vectors are necessary to define the five independent elements of each alignment tensor. The dynamical content contained within the RDC data is encapsulated by a generalized order parameter, S_{RDC}^2, which possesses dynamic information on the picosecond to millisecond time-scale, which includes the supra-τ_c range (Figure 1). Within the framework of ensemble averaging, Equations (11) and (12) become:

$$\mathbf{D} = \langle \mathbf{B} \rangle \langle \mathbf{A} \rangle \tag{13}$$

$$\langle \mathbf{A} \rangle = \langle \mathbf{B} \rangle^{+}\mathbf{D} \tag{14}$$

There are two principal schemes for extracting the structural and dynamic content from RDC data measured in at least five linearly independent alignment media, namely the Model Free Analysis (MFA) [72] and the Direct Interpretation of Dipolar Couplings (DIDC) [68]. Before delving into the details concerning these model free approaches, we discuss a necessary caveat for the implementation

of this methodology and how to assess the quality of the RDC data, as well as the sampling of the five-dimensional space.

The fundamental assumption for both the MFA and DIDC approaches is that the internal protein dynamics for each inter-nuclear vector is uncorrelated with alignment tensor. Thus, a single average alignment tensor can be utilized for each medium. Molecular dynamics simulations indicate that this assumption is true for secondary structural elements, yet ⟨**B**⟩ and ⟨**A**⟩ dynamics may be correlated for the most mobile regions of a protein [73,74]. In the case of intrinsically disordered proteins [75,76], multi-domain proteins [77,78], and extended nucleic acid structures [48,79], internal conformational dynamics couples with the alignment tensor. After realizing that even intrinsically disordered proteins exhibit RDCs [80,81], Blackledge and co-workers have developed strategies for interpreting RDCs measured for intrinsically disordered proteins and the reader is referred to the following papers on the subject [82–84]. RDCs measured for multi-domain proteins report on both inter-nuclear vector dynamics and inter-domain dynamics that result in changes in molecular alignment [85]. One avenue to de-correlate these two processes is to use internal paramagnetic alignment where one domain is preferentially aligned in the magnetic field [78,86]. Though the focus of this section is assessing inter-nuclear vector dynamics via RDCs obtained from external alignment media, we direct the interested reader to these papers on utilizing paramagnetic tagging for the determination of structure, inter-domain orientation and dynamics with RDCs from the groups of Ubbink [87,88], Bertini [78,89,90], Otting [91,92], Byrd [93,94], and Schwalbe [95,96]. As for aligning extended nucleic acid structures, such as RNA, the laboratory of Al-Hashimi has developed a novel strategy of elongating RNA helices [97]. In this situation, the extended RNA structure dominates the molecular alignment and the internal dynamics of the RNA helix no longer contributes to the overall alignment of the biomolecule [98].

When analyzing RDC data, a fundamental assumption that is made concerns the uncorrelatedness of the inter-nuclear dynamics and the alignment process; hence the averages of ⟨**B**⟩ and ⟨**A**⟩ are independent of each other. This assumption can be tested with the Self-Consistency of Dipolar Couplings Analysis (SECONDA) [99,100]. SECONDA attempts to quantitate the degree of structural heterogeneity for the measured protein over at least 6 different alignment media. The analysis only requires RDC data as input, without structural data or alignment tensor information. In principal, perfectly homogenous behavior suggests that the internal structural dynamics are not influenced by the variations in the alignment process, in temperature or in pH. Furthermore, the homogeneity can be quantified on a per residue basis. A covariance matrix is created from the RDC data and from a principal component analysis or SVD of the covariance matrix the degree of structural heterogeneity is assessed from the resulting singular values. The first five singular values contain the structural and dynamic content encompassed within the RDC data. The other singular values indicate the degree of structural and dynamic heterogeneity, noise, and systematic errors resulting in singular values that are not equal to zero. The SECONDA gap is a measure of the self-consistency and homogeneity of the RDC data set, which is the ratio of the 5th and 6th singular value.

The degree in which the five dimensional space is being sampled can be quantified from SVD [68,101]. SVD of the five independent elements of each alignment tensor within ⟨**A**⟩ yields five singular values. The ratio of the first to the fifth singular value indicates the strength of the contribution from the strongest and weakest dimensions being sampled by the RDC data. This parameter is called the condition number. A value of one indicates that each dimension is being sampled equally. In the case

of ubiquitin where 36 RDC data sets were available the average condition number was 6.3 [102]. Residues 22, 31, 46, 69, and 73 were removed from this 36 RDC data set, since they possessed condition numbers larger than 10.

We will focus our discussion on the extraction of structural and dynamic content from RDC data on the similar nature of both the MFA and DIDC analysis and how they are unified within the context of the standard tensorial analysis [103]. Beginning with the MFA, five independent alignment media are necessary to calculate the five independent elements of the RDC tensor for each inter-nuclear vector, as well as *a priori* knowledge of the protein structure [72,101]. With the alignment tensor information, the averages over the second rank spherical harmonics describing the mean orientations of the vectors, contained within the RDC tensor, provide the desired structural and dynamic content. The alignment tensor parameters taken from the alignment frame (AF), $\{D_a, R, \alpha, \beta, \gamma\}_l$, are used to construct the $\langle \mathbf{F} \rangle$ matrix which is needed to derive the five dynamically averaged second order spherical harmonics:

$$\langle Y_{2,0}(\theta_k^{MF}, \phi_k^{MF}) \rangle = \sqrt{\frac{5}{16\pi}} \langle 3\cos^2\theta_k^{MF} - 1 \rangle \tag{15}$$

$$\langle Y_{2,\pm1}(\theta_k^{MF}, \phi_k^{MF}) \rangle = \mp\sqrt{\frac{15}{8\pi}} \langle e^{\pm i\phi_k^{MF}} \cos\theta_k^{MF} \sin\theta_k^{MF} \rangle \tag{16}$$

$$\langle Y_{2,\pm2}(\theta_k^{MF}, \phi_k^{MF}) \rangle = \sqrt{\frac{15}{32\pi}} \langle e^{\pm 2i\phi_k^{MF}} \sin^2\theta_k^{MF} \rangle \tag{17}$$

Utilizing the following relationships,

$$\langle Y_{2,0}(\theta_{k,l}^{AF}, \phi_{k,l}^{AF}) \rangle = \sqrt{\frac{5}{16\pi}} \langle 3\cos^2\theta_{k,l}^{AF} - 1 \rangle \tag{18}$$

$$\langle Y_{2,2}(\theta_{k,l}^{AF}, \phi_{k,l}^{AF}) \rangle + \langle Y_{2,-2}(\theta_{k,l}^{AF}, \phi_{k,l}^{AF}) \rangle = 2\sqrt{\frac{15}{32\pi}} \langle \sin^2\theta_{k,l}^{AF} \cos 2\phi_{k,l}^{AF} \rangle \tag{19}$$

Equation (9) is reformulated in terms of dynamically averaged second order spherical harmonics

$$D_{k,l}^{exp} = A_{zz,l}^{PAS} \sqrt{\frac{4\pi}{5}} \left[\langle Y_{2,0}(\theta_{k,l}^{AF}, \phi_{k,l}^{AF}) \rangle + \sqrt{\frac{3}{8}} R_l \left(\langle Y_{2,2}(\theta_{k,l}^{AF}, \phi_{k,l}^{AF}) \rangle + \langle Y_{2,-2}(\theta_{k,l}^{AF}, \phi_{k,l}^{AF}) \rangle \right) \right] \tag{20}$$

The $\langle \mathbf{F} \rangle$ matrix functions in a similar way to $\langle \mathbf{A} \rangle$ and relates the measured RDCs to the spherical harmonics defined in the MF by a Wigner rotation from the MF to the AF:

$$\frac{D_{k,l}^{exp}}{A_{zz,l}^{PAS}} = \sum_{M=-2}^{2} F_{l,M} \langle Y_{2,M}(\theta_k^{MF}, \phi_k^{MF}) \rangle \tag{21}$$

with:

$$F_{l,M} = \sqrt{\frac{4\pi}{5}}\left[D^2_{M0}(\alpha_l,\beta_l,\gamma_l) + \sqrt{\frac{3}{8}}R_l(D^2_{M2}(\alpha_l,\beta_l,\gamma_l) + D^2_{M-2}(\alpha_l,\beta_l,\gamma_l))\right]$$

$$= \sqrt{\frac{4\pi}{5}}\left[e^{-iM\alpha_l}d^2_{M0}(\beta_l) + \sqrt{\frac{3}{8}}R_l\left(e^{-iM\alpha_l}d^2_{M2}(\beta_l)e^{-i2\gamma_l} + e^{-iM\alpha_l}d^2_{M-2}(\beta_l)e^{i2\gamma_l}\right)\right] \quad (22)$$

In analogy to the component definition from Equations (13) and (14), $\langle\mathbf{Y}\rangle$ is a K x 5 matrix containing the dynamically averaged spherical harmonics in the MF and $\langle\mathbf{F}\rangle$ is a 5 x L matrix containing the alignment tensor information. Refined structural coordinates are determined directly from the RDCs and alignment information:

$$\langle\mathbf{Y}\rangle_{\mathbf{refined}} = \mathbf{D}_{\mathbf{normalized}}\langle\mathbf{F}\rangle^{+} \quad (23)$$

In order to normalize the contributions of each alignment condition to the calculation of refined structural coordinates, $\mathbf{D}_{\mathbf{normalized}}$ represents $\frac{D^{exp}_{k,l}}{A^{PAS}_{zz,l}}$ which results in the condition number being lower than in the unnormalized case. In other words, this normalization helps to even out the contributions of each RDC set to the calculation of $\langle\mathbf{Y}\rangle_{\mathbf{refined}}$. Each row of $\langle\mathbf{Y}\rangle_{\mathbf{refined}}$ is used to determine $S^2_{RDC,k}$:

$$S^2_{RDC,k} = \frac{4\pi}{5}\sum_{M=-2}^{2}\langle Y_{2,M}(\theta^{MF}_k,\phi^{MF}_k)\rangle\langle Y^*_{2,M}(\theta^{MF}_k,\phi^{MF}_k)\rangle \quad (24)$$

From the dynamically averaged spherical harmonics, the dynamically averaged orientations for each inter-nuclear vector, $(\theta^{MF}_{avg,k},\phi^{MF}_{avg,k})$, can be obtained. Maximizing $\langle Y_{2,0}(\theta^{VF}_k,\phi^{VF}_k)\rangle$ places the z-axis of the vector's axis system, termed the vector frame (VF), in the center of the inter-nuclear vector's orientational distribution:

$$\max\langle Y_{2,0}(\theta^{VF}_k,\phi^{VF}_k)\rangle = \sum_{M=-2}^{2} D_{M,0}(\phi^{MF}_{avg,k},\theta^{MF}_{avg,k},0)\langle Y_{2,M}(\theta^{MF}_k,\phi^{MF}_k)\rangle$$

$$= \sqrt{\frac{4\pi}{5}}\sum_{M=-2}^{2} Y_{2,-M}(\theta^{MF}_{avg,k},\phi^{MF}_{avg,k})\langle Y_{2,M}(\theta^{MF}_k,\phi^{MF}_k)\rangle \quad (25)$$

The terms $\langle Y_{2,\pm1}(\theta^{MF}_k,\phi^{MF}_k)\rangle$ vanish in the VF and $\langle Y_{2,\pm2}(\theta^{MF}_k,\phi^{MF}_k)\rangle$ possesses information on the amplitude of anisotropy, η_k, and the orientation of anisotropic motions, $\phi_k^{'}$:

$$\eta_k = \sqrt{\frac{\sum_{M=-2,2}\langle Y_{2,M}(\theta^{VF}_k,\phi^{VF}_k)\rangle\langle Y_{2,-M}(\theta^{VF}_k,\phi^{VF}_k)\rangle}{\sum^2_{M=-2}\langle Y_{2,M}(\theta^{VF}_k,\phi^{VF}_k)\rangle\langle Y_{2,-M}(\theta^{VF}_k,\phi^{VF}_k)\rangle}} \quad (26)$$

$$\phi_k^{'} = \frac{1}{2}\arctan\frac{\langle Y_{2,2}(\theta^{VF}_k,\phi^{VF}_k)\rangle - \langle Y_{2,-2}(\theta^{VF}_k,\phi^{VF}_k)\rangle}{i(\langle Y_{2,2}(\theta^{VF}_k,\phi^{VF}_k)\rangle + \langle Y_{2,-2}(\theta^{VF}_k,\phi^{VF}_k)\rangle)} \quad (27)$$

It should be noted that $S^2_{RDC,k}$ is the same in any frame, thus:

$$S^2_{RDC,k} = \frac{4\pi}{5}\sum_{M=-2}^{2}\langle Y_{2,M}(\theta^{VF}_k,\phi^{VF}_k)\rangle\langle Y^*_{2,M}(\theta^{VF}_k,\phi^{VF}_k)\rangle \quad (28)$$

which is equivalent to Equation (24).

With the DIDC approach, structural input is not required in the calculation of the inter-nuclear vector's structural and dynamic content [68]. In concordance with Equation (23):

$$\langle \mathbf{B} \rangle_{\mathbf{refined}} = \mathbf{D}\langle \mathbf{A} \rangle^{+} + \mathbf{B}[\mathbf{1} - \langle \mathbf{A} \rangle \langle \mathbf{A} \rangle^{+}] \tag{29}$$

where $\langle \mathbf{B} \rangle_{\mathbf{refined}}$ can be calculated without extracting each set of $\{D_a, R, \alpha, \beta, \gamma\}_l$. A key difference between the MFA and DIDC is the requirement of normalizing $\mathbf{D}$ and $\langle \mathbf{A} \rangle$. In the current implementation of DIDC, these parameters are not normalized, which will lead to some discrepancies between RDC analysis utilizing the MFA and the DIDC. Neglecting this normalization will lead to a disproportionate contribution of the stronger alignment media to the calculation of the refined structural coordinates. We propose the following modification of Equation (29) for the DIDC approach when seeking a direct correspondence between both methods:

$$\langle \mathbf{B} \rangle_{\mathbf{refined}} = \mathbf{D}_{\mathbf{normalized}} \langle \mathbf{A} \rangle^{+}_{\mathbf{normalized}} + \mathbf{B}[\mathbf{1} - \langle \mathbf{A} \rangle \langle \mathbf{A} \rangle^{+}] \tag{30}$$

where $\mathbf{D}_{\mathbf{normalized}}$ and $\langle \mathbf{A} \rangle_{\mathbf{normalized}}$ represent the RDCs and alignment tensors divided by $A^{PAS}_{zz,l}$.

The unification of both the MFA and the DIDC is readily apparent when looking at the relationship between $\langle \mathbf{B} \rangle$ and $\langle \mathbf{Y} \rangle$. Recalling Equation (6), the following relationships are established in order to construct $B^{(2)}_k$ [34]:

$$b_{zz,k} = \sqrt{\frac{4\pi}{5}} \langle Y_{2,0}(\theta^{MF}_k, \phi^{MF}_k) \rangle \tag{31}$$

$$\frac{1}{\sqrt{3}}\left(b_{xx,k} - b_{yy,k}\right) = \sqrt{\frac{1}{2}}\sqrt{\frac{4\pi}{5}}\left[\langle Y_{2,-2}(\theta^{MF}_k, \phi^{MF}_k) \rangle + \langle Y_{2,2}(\theta^{MF}_k, \phi^{MF}_k) \rangle\right] \tag{32}$$

$$\frac{2}{\sqrt{3}} b_{xz,k} = \sqrt{\frac{1}{2}}\sqrt{\frac{4\pi}{5}}\left[\langle Y_{2,-1}(\theta^{MF}_k, \phi^{MF}_k) \rangle - \langle Y_{2,1}(\theta^{MF}_k, \phi^{MF}_k) \rangle\right] \tag{33}$$

$$\frac{2}{\sqrt{3}} b_{yz,k} = i\sqrt{\frac{1}{2}}\sqrt{\frac{4\pi}{5}}\left[\langle Y_{2,-1}(\theta^{MF}_k, \phi^{MF}_k) \rangle + \langle Y_{2,1}(\theta^{MF}_k, \phi^{MF}_k) \rangle\right] \tag{34}$$

$$\frac{2}{\sqrt{3}} b_{xy,k} = i\sqrt{\frac{1}{2}}\sqrt{\frac{4\pi}{5}}\left[\langle Y_{2,-2}(\theta^{MF}_k, \phi^{MF}_k) \rangle - \langle Y_{2,2}(\theta^{MF}_k, \phi^{MF}_k) \rangle\right] \tag{35}$$

In 2012, Meirovitch *et al.* made the following connection between maximizing $\langle Y_{2,0}(\theta^{VF}_k, \phi^{VF}_k) \rangle$ and defining each inter-nuclear vector in a unique principal axis system [103]. The resulting eigenvalues $(B^{PAS}_{mm,k})$ contain the dynamic information for each vector $\left(S^2_{RDC,k}, \eta_k\right)$, while the eigenvectors,$\left(B^{EV}_{mn,k}\right)$, encompass the bond orientations $(\theta^{MF}_k, \phi^{MF}_k)$ and the direction of the anisotropic local motion (ϕ'_k). The following equations detail how the dynamic parameters are calculated from $B^{PAS}_{mm,k}$. The Saupe order parameters are defined as:

$$S^2_{0,k} = B^{PAS}_{zz,k} = \sqrt{\frac{4\pi}{5}} \langle Y_{2,0}(\theta^{PAS}_k, \phi^{PAS}_k) \rangle \tag{36}$$

$$S_{2,k}^2 = \sqrt{\frac{2}{3}}(B_{xx,k}^{PAS} - B_{yy,k}^{PAS}) = \sqrt{\frac{4\pi}{5}}\left[\langle Y_{2,2}(\theta_k^{PAS}, \phi_k^{PAS})\rangle + \langle Y_{2,-2}(\theta_k^{PAS}, \phi_k^{PAS})\rangle\right] \tag{37}$$

$$S_{RDC,k}^2 = \left(B_{zz,k}^{PAS}\right)^2 + \frac{1}{3}\left(B_{xx,k}^{PAS} - B_{yy,k}^{PAS}\right)^2 = \left(S_{0,k}^2\right)^2 + \frac{1}{2}\left(S_{2,k}^2\right)^2 \tag{38}$$

$$\eta_k^{PAS} = \sqrt{\frac{\frac{1}{3}\left(B_{xx,k}^{PAS} - B_{yy,k}^{PAS}\right)^2}{S_{RDC,k}^2}} = \sqrt{\frac{\frac{1}{2}\left(S_{2,k}^2\right)^2}{S_{RDC,k}^2}} \tag{39}$$

For each inter-nuclear vector, $(\theta_k^{MF}, \phi_k^{MF})$ and $\phi_k^{'}$ are extracted from the transpose of the resulting $B_{mn,k}^{EV}$ matrix:

$$\phi_k^{MF} = \arctan\left[B_{xz,k}^{EV}, B_{yz,k}^{EV}\right],\ \theta_k^{MF} = \arccos\left[B_{zz,k}^{EV}\right],\ \phi_k^{'} = \arctan\left[-B_{zx,k}^{EV}, B_{zy,k}^{EV}\right]. \tag{40}$$

Both the MFA and DIDC methods have been incorporated into iterative schemes with the goal of improving the accuracy of the alignment tensor calculation by reducing the effects of the structural noise, termed the Self-Consistent RDC based MFA (SCRM) [102], iterative DIDC [104] and the Optimized RDC-based Iterative and Unified Model-free analysis (ORIUM) [89]. The iterative schemes achieve this by using the refined dynamically averaged coordinates as input for additional runs of either MFA or DIDC. Interestingly, ORIUM is the only iterative procedure that can begin with random coil input as the starting structural coordinates and extract the same structural and dynamic information calculated from an x-ray structure used as the beginning structural input [105]. This result shows that the iterative ORIUM scheme tolerates a significant amount of structural noise and has the potential be implemented in refinement of conformational ensembles.

A final consideration when determining the dynamic parameters from RDC data is that the actual magnitude of $A_{zz,l}^{PAS}$ or $D_{a,l}$ is not known, which will lead to S_{RDC}^2 values being only relative in nature to the true absolute value [27,72]. The other alignment tensor parameters $\{R, \alpha, \beta, \gamma\}_l$ are unaffected by the reduction in the magnitude of $D_{a,l}$. The correct scaling parameter, termed $S_{overall}$, is crucial for distinguishing sub- and supra-τ_c motion. All three iterative schemes have addressed this issue in different manners. In the iterative DIDC, order parameters are scaled relative to the largest $S_{RDC,unscaled}^2$ leaving one order parameter equal to one [68,104]. Sub- and supra-τ_c motion happening for each vector equally will not be detected by this approach, which will underestimate the motion. With the MFA/SCRM procedure, $S_{RDC,unscaled}^2$ is scaled relative to the Lipari-Szabo order parameters (S_{LS}^2) calculated for each residue [27,102], as long as S_{LS}^2 are available for the inter-nuclear vectors being analyzed. This approach as been successfully applied to ubiquitin, however, supra-τ_c motion affecting all nuclei equally will not be picked up by this method. Finally, ORIUM uses the inter-nuclear vector's motional variance, which is directly related to the resulting eigenvalues calculated from diagonalization of $B_k^{(2)}$ into a local axis system. By definition, variance cannot be negative, and therefore, a uniform scaling parameter, $S_{overall}$, is necessary to insure that the variance for each inter-nuclear vector about each of the three principal axes is positive. The advantage of this method is that $S_{overall}$ is derived based on variances of a single type of RDC without needing S_{LS}^2 as a constraint, and hence does not possess any time-scale bias. Yet, it should be noted that $S_{overall}$ determined by this procedure could underestimate motion if there is a uniform sub- or supra-τ_c motion affecting all inter-nuclear vectors equally.

2.4. Gaussian Axial Fluctuation Model

Brüschweiler and co-workers developed a model, termed the Gaussian Axial Fluctuation model (GAF), describing rotational motion of the peptide plane around the axis defined by Cα(*i*-1) and Cα(*i*) [106–108]. The original observation for this type of motion comes from NMR spin relaxation measurements as well as molecular dynamics simulations, where crankshaft type motions along this axis were observed. Blackledge and co-workers have adapted this model for the use with RDC data, which spans up to the millisecond time-scale [109–111]. The amount of this motion is encapsulated in the angular standard deviation (σ) about three orthogonal axes defined by the peptide plane. In the simplest formulation, considering motion about the axis defined by Cα(*i*-1) and Cα(*i*), the model is considered (ortho-GAF) and σ is incorporated into Equation (6) as follows:

$$D_{k,l}^{ortho-GAF} = \frac{D_{ij}^{max}}{2}\left\{\frac{A_{zz}^{PAS}}{4}\left[s_1(3\cos^2\beta - 1) + 3s_2(\sin^2\beta\cos 2\alpha)\right] + \frac{(A_{xx}^{PAS} - A_{yy}^{PAS})}{4A_{xx}^{PAS}}\left[s_1\sin^2\beta\cos 2\gamma + \right.\right.$$

$$2s2\cos 4\beta 2\cos 2\delta 1 + \sin 4\beta 2\cos 2\delta 2, \quad (41)$$

where:

$$s_1 = 1 + 3e^{-2\sigma^2}, s_2 = 1 - e^{-2\sigma^2}, \delta_1 = \alpha + \beta, \delta_2 = \alpha - \gamma. \quad (41)$$

Here, α, β, γ represent the Euler angles describing the transformation into the peptide plane's frame, where the z-axis points along the direction of the N-H^N bond and the x-axis orthogonal to the peptide plane. This rotation is similar to putting the N-H^N bond in the local principal axis system described above. It should be noted that the Cα(*i*-1) and Cα(*i*) axis is tilted away from the y axis by 11 degrees.

As is this case with RDCs measured in alignment media with unknown absolute magnitude, the GAF method also requires a scaling factor, which has been addressed with the structure-free (SF) GAF approach [112]. The methodology treats each peptide plane as an independent entity, the only requirement being the starting coordinates for a representative peptide plane. RDC data measured in multiple alignment media for the N-H^N, C'N, C'- H^N, and C'-Cα were used to fit for the residue specific $\alpha, \beta, \gamma, \sigma_z, \sigma_y, \sigma_x$ and the alignment condition specific A_{zz}^{PAS}. This procedure was most effective when using the full 3D-GAF model. For ubiquitin, a comparison of S_{RDC}^2 derived from the SCRM [102] approach of constraining with S_{LS}^2 with the SF-GAF method S_{RDC}^2 displayed remarkable agreement.

2.5. Supra-τ_c Dynamics Determined from RDCs is linked to Molecular Recognition

The potential linkage of experimentally extracted inter-nuclear vector dynamics within the supra-τ_c range to molecular recognition has been investigated for three proteins: ubiquitin (SCRM [102]/ SF-GAF [54]/ORIUM [105]), GB3 (iterative DIDC [45]/3D-GAF [111], ORIUM [105]) and SH3 (3D-GAF [113]). Amplitudes of supra-τ_c motion can be readily quantified from knowledge of S_{RDC}^2 and S_{LS}^2:

$$S_{\text{supra}-\tau_c}^2 = \frac{S_{RDC}^2}{S_{LS}^2} \quad (42)$$

For all three proteins, additional motions resulting from slower time-scale dynamics are present. Furthermore, in the case of ubiquitin, there exists a significant amount of motion for the side-chain

methyl groups [114], while such studies have not yet been conducted for the other two proteins. The connection to molecular recognition rests in the observation that for some residues possessing significant $S^2_{\mathrm{supra}-\tau_c}$ are involved with binding to interaction partners. When considering the interacting partners SH3 and ubiquitin, they both appear to possess a significant amount of supra-τ_c motion at their respective binding interfaces [102,113].

Molecular dynamics (MD) simulations restrained with or validated against RDC data is an approach to develop an ensemble of structures that best represents the ground state ensemble of the protein. Recently, RDC data was used as a restraint in MD simulations of ubiquitin. A principal component analysis of the resulting ensemble demonstrated that ubiquitin samples the same conformational space as all conformers captured to date in crystal structures of ubiquitin complexes [28]. These findings support the concept of conformational selection, specifically that amplitudes of motion or dynamics resulting from conformational inter-conversion on the supra-τ_c scale are limiting the on-rates for complex formation [115]. For ubiquitin, a majority of these conformational dynamics are concentrated in a single collective mode described by a pincer-like motion. To alleviate the entropic costs associated with sampling conformers along the pincer-like trajectory, another ubiquitin conformational ensemble predicts a significant amount of correlated motions, determined from long range ϕ/ψ dihedral correlations [116]. These findings demonstrate the power of using RDC data to refine ensembles containing dynamic information on the supra-τ_c scale.

Accelerated molecular dynamics (AMD) is another strategy for utilizing RDC data in the generation of a conformational ensemble possessing dynamics up to the millisecond time-scale [117]. In AMD, the energy barriers between the many conformational states of a protein ensemble are lowered, allowing the AMD simulation to cover conformational space that potentially exists on longer time-scales. From here, a canonical ensemble can be generated from a Boltzmann reweighting of each ensemble member. The AMD approach has been employed with several protein systems, including GB3 [118], ubiquitin [119], thrombin [120,121], and IκBα [122]. In all cases, the AMD ensembles were cross-validated with RDC data, then order parameters were calculated. Supra-τ_c motion is also present with the AMD method, suggesting, at least for systems as large as thrombin and IκBα, a common time-scale of supra-τ_c motion may be present for all proteins.

As this section has demonstrated, RDC data encompasses important information regarding the amplitudes of motion spanning the supra-τ_c scale. The next step is to assign a specific rate to this motion. Are these dynamics related to conformational inter-conversion within the ground state ensemble and, if so, what is the time-scale of this process? A powerful technique to potentially answer this question comes from relaxation dispersion measurements. The next section reviews the progress that has been made linking RDC extracted supra-τ_c scale dynamics to a specific rate describing the actual process of conformational inter-conversion.

3. Kinetics from the Supra-τ_c Range

3.1. Sub-τ_c Relaxation is Limited to the Overall Tumbling Time

Conventional NMR relaxation focuses on backbone ^{15}N nuclei and we will limit our discussion to this nucleus type [123,124], although, a plethora of experiments have been developed that can probe the relaxation processes of other nuclei [125–130]. Commonly applied NMR experiments measure the longitudinal and transverse relaxation rates, R_1 and $R_{2,0}$, respectively [124]. These intrinsic relaxation parameters report on local oscillating magnetic fields that are generated due to dipolar interactions between the ^{15}N nucleus and its attached amide proton (dipole-dipole coupling) and from magnetic fields generated due to a nucleus electron cloud's orientation with the static magnetic field (chemical shift anisotropy) [131]. These local magnetic fields are reoriented because of molecular tumbling which for proteins occurs in the nanosecond range and demarcated by the characteristic lifetime called the overall rotational correlation time (τ_c). These relaxation rates are described by spectral density type functions that are evaluated at characteristic frequencies, which report on transitions that drive nuclei back to equilibrium. These frequencies occur at zero, $\omega_{H/N}$, and $\omega_H \pm \omega_N$ where ω_X is the Larmor frequency for either ^1H or ^{15}N nuclei [131–133]. However, since these relaxation rates depend on fluctuations of dipolar couplings that are averaged by the molecular reorientation occurring with the correlation time τ_c, only motions up to that time are accessible, *i.e.* motions that are slower than the inverse correlation time are not reflected in these relaxation rates. This range of motion faster than the inverse correlation time is called the sub-τ_c window. The experiments that probe these relaxation rates function by probing inphase coherences of the type $N_{x,y}$ and N_z for $R_{2,0}$ and R_1, respectively [1,134], from which the longevity of these coherences is queried by observing their rate of decay which is extracted using a two parameter exponential decay function [135].

A broad range of information can be retrieved from the measurement of relaxation rates. The ratio of $R_{2,0}$ and R_1 can be used to determine τ_c itself [124], and many insights into local molecular flexibility can be attained by performing a Model-Free analysis (MF) [136,137]. The MF formalism allows the extraction of an order parameter that quantifies the spatial flexibility of a given inter-nuclear vector. This parameter can also be used as a proxy for conformational entropy [138–141]. An extended MF formalism has been developed for the characterization of internal motion occurring from two distinct time-scales within the sub-τ_c range [142]. The local and overall rotational anisotropy [143] of a macromolecule and the orientations of modular proteins [144,145] can also be ascertained from such data. Although insight into motion from the sub-τ_c range has given input into finer molecular motions, some biologically relevant processes cannot be assessed with these types of measurements due to the time-scale limitation.

The kinetic characterization for biologically relevant processes like protein folding [146–149], enzymatic turnover events [150–154], and molecular recognition [155–157] are inaccessible by conventional sub-τ_c relaxation techniques. Instead, NMR based relaxation dispersion (RD) experiments have emerged as a successful tool to explore these processes [1,158–160]. Fifty years ago, the concept of RD was applied for the measurement of the proton transfer rate between trimethylammonium and trimethylamine [161]. The success of these experiments is directly related to their ability to exploit the phenomenon of conformational exchange. Conformational exchange occurs when the electronic

environment of a nucleus is perturbed due to its own motion or from its surroundings. This motion in turn modulates a nuclei's isotropic chemical shift (ω) thereby causing the generation of alternatively populated coherences [159,162]. These variously populated states also interconvert with a given lifetime (τ_{ex}) whose smallest observable value is limited by the experimental conditions. The effect of conformational exchange creates a dephasing in the transverse plane that is appended to $R_{2,0}$. This dephasing creates an effective transverse relaxation rate, $R_{2,eff} = R_{2,0} + R_{ex}$ where R_{ex} is a contribution of relaxation due to conformational exchange.

The lifetime for a conformational exchange event is governed by the chemical shift time-scale [163]. Traditionally, the process is defined to be either in the slow, intermediate, or fast regime. These regimes are separated based on the inverse ratio of the product between the chemical shift difference between populated states ($\Delta\omega$) and τ_{ex} ($(\Delta\omega\,\tau_{ex})^{-1}$) which for slow, intermediate, and fast processes take on the values of < 1, ≈ 1, and > 1, respectively [163]. For processes that may take place in the supra-τ_c range (10s of μs and faster) motion is in the fast regime and therefore a given resonance position will represent a population weight of all assumed states. Since conformational exchange is governed by perturbations in ω, the line width of an NMR lineshape is affected during a period of free-precession. Assuming a two-state model, the contribution to the line width due to fast exchange is $R_{ex} = p_A p_B \Delta\omega^2 \tau_{ex}$ in which p_A is the population of the major state ($p_B = 1 - p_A$) [159,162]. The next section explores how RD experiments work to disentangle these parameters that modify transverse relaxation.

3.2. Relaxation Dispersion Experiments

The two most commonly invoked RD experiments are the transverse-rotating frame relaxation ($R_{1\rho}$) [160,164] and Carr-Purcell-Meiboom-Gill (CPMG) [165,166] experiments. CPMG experiments have grown large popularity to be able to study lowly populated intermediates for some systems [147,157,167]. However, RD can also be used to probe the ground states of a protein as well [115]. Other methods have also been proposed for RD experiments [168,169]. Although, the dependence of conformational exchange differs between the $R_{1\rho}$ and CPMG techniques [1,170], the phenomenological concept is the same. In both cases a relaxation rate is monitored as a function of the rate at which a given magnetization coherence can be refocused. CPMG experiments vary the degree of refocusing by changing 180° pulse repetition rates [171–174], and $R_{1\rho}$ experiments use radio frequency pulses with varying amplitudes and frequency offsets that effectively constrain (spin-lock) a given magnetization coherence [160]. The amplitude of a given spin-lock pulse is denoted as ν_{RF}. However, due to technical limitations, CPMG experiments, when performed on ^{15}N nuclei, permit the observation of motions with a τ_{ex} of up to ~150 μs [135]. $R_{1\rho}$ experiments were limited to a time resolution of 40 μs, but now ν_{RF} values permit the observation of kinetic events up to 25 μs (*vide infra*) which has made this NMR experiment a well suited candidate to access kinetic information from the supra-τ_c range.

Figure 2. Illustrative schematic describing transverse rotating frame experiments ($R_{1\rho}$) for the measurement of two-state conformational exchange events for NMR active nuclei. As states A and B interconvert with some lifetime (τ_{ex}) they have a phase separation of $\Delta\omega$. The length of each vector (arrow tipped lines) denotes the effective field that each populated coherence possesses. The effective field, or length of each vector, is governed by experimental parameters, namely the offset (Ω) and ν_{RF}, where Ω is the difference between the resonance frequency for a given nucleus and the frequency at which ν_{RF} is applied. The effective field can be calculated as $\omega_{eff} = \sqrt{(2\pi\Omega)^2 + (2\pi\upsilon_{RF})^2}$ (rad s^{-1}). The incomplete refocusing of state B (vector diagram on the left) leads to a dephasing of the magnetization, which translates to a larger relaxation rate. Upon sufficient refocusing of both magnetization vectors (vector diagram on the right) the relaxation rate decreases to $R_{2,0}$. The cones directly reflect the size of the nutation generated from the applied spin-lock field. In the fast regime, the dependence of $R_{2,eff}$ with an increasing ν_{RF} gives a Lorentzian profile [Equation (44)]. If no conformational exchange exists, then $R_{2,eff}$ remains constant for all applied ν_{RF} values.

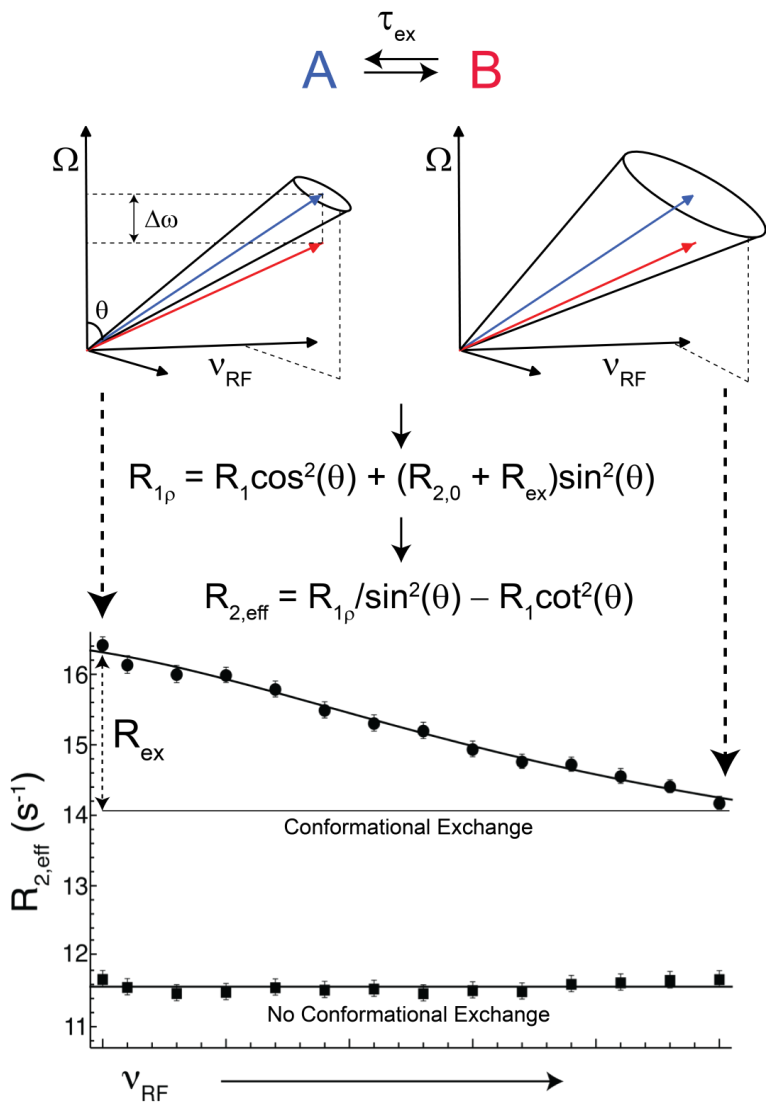

3.3. Off/On-Resonance $R_{1\rho}$

Off- and on-resonance $R_{1\rho}$ experiments have been applied to a variety of topics related to the study of internal molecular motions such as hinge and loop displacements [175,176], fast folding events [177], structural configurations that can be assumed in solution by DNA/RNA [178,179], and molecular recognition events [115]. $R_{1\rho}$ experiments can be used as a type of RD experiment because they create "dispersion" by monitoring a nuclei specific relaxation rate as a function of the amplitude of a spin-lock field (ν_{RF}) and/or by manipulation of the offset frequency (Ω). The transverse rotating frame relaxation rate is dependent on the intrinsic R_1, $R_{2,0}$, and if conformational exchange exists R_{ex}. In the off-resonance $R_{1\rho}$ scenario, populated coherences are rotated away from the static magnetic field by some tilt angle (θ), where the magnetization is locked and thereby begins to precess with the applied field (Figure 2). The tilt angle is an experimentally controlled parameter, $\theta = \tan^{-1}(\nu_{RF}/\Omega)$ where ν_{RF} and Ω are the amplitude of the employed spin-lock (Hz) and the frequency difference between the resonance position of a given nuclei and the frequency at which ν_{RF} is applied, respectively. The overall magnitude of a spin-lock field is called the effective field ($\omega_{eff} = \sqrt{(2\pi\nu_{RF})^2 + (2\pi\Omega)^2}$ (rad s^{-1})). If an interconversion event exists, then assuming a two-state process, the populated coherences will be differentially spin-locked (Figure 2). At this point, the alternatively populated coherence is not sufficiently refocused and dephasing leads to an elevated effective relaxation rate ($R_{2,eff}$) (Figure 2). As ω_{eff} is sufficiently increased to encompass the exchanging magnetization vectors, the relaxation rate decreases to $R_{2,0}$ or to the point at which the exchange contribution to $R_{2,eff}$ is quenched (Figure 2).

The equation that describes off-resonance $R_{1\rho}$ is given in Figure 2. In order to isolate the effect of conformational exchange, it is convenient to visualize the contribution of R_{ex} by either converting off-resonance $R_{1\rho}$ data to $R_{2,eff}$ (Figure 2) or by performing $R_{1\rho}$ experiments on-resonance ($\theta = \pi/2$) whereby the dependence of R_1 and the tilt angle are removed. If motion exists in the fast regime, then this creates an addendum to $R_{1\rho}$ that is given by:

$$R_{ex} = \frac{p_A p_B \Delta\omega^2 \tau_{ex}}{1 + (\tau_{ex}\omega_{eff})^2} \tag{43}$$

However when the motion is fast, then information between the populations and $\Delta\omega$ cannot be separated and therefore only the product is retained. This is called the conformational amplitude of the process and is denoted as Φ_{ex}. Comparing the dependence of R_{ex} between $R_{1\rho}$ and CPMG type experiments it can be seen that their dependence is similar (Figure 3). The 180° pulse repetition rate (ν_{CPMG}) can be equated to ν_{RF} using relations derived from Ishima *et al.* ($\frac{\sqrt{3}}{6}\pi\nu_{RF} = \nu_{CPMG}$) [180].

Figure 3. Dependence of R_{ex} monitored by $R_{1\rho}$ (solid black line) and CPMG (dashed black line) experiments. The dashed black line was created using the Carver-Richards model [181] which is applicable for CPMG experiments, and the solid black curve calculated using Equation (44). The exchange parameters τ_{ex}, p_B, and $\Delta\omega$, were set to 150 μs, 5 %, and 61 Hz, respectively.

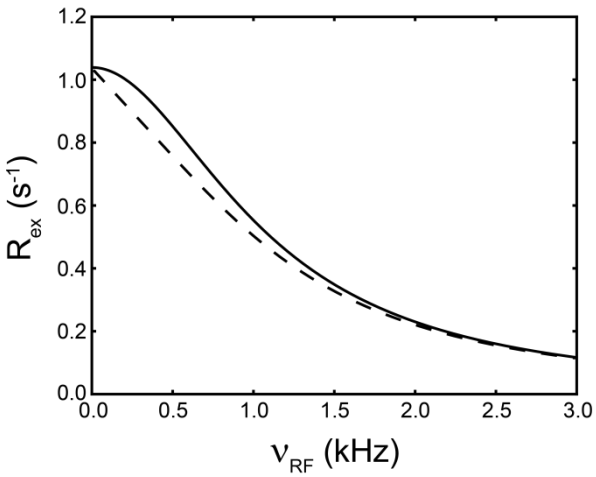

It is also important to note that, similar to CPMG experiments, theoretical formalisms and experiments have been reported in which $R_{1\rho}$ can be applied outside of the fast regime [182–184]. Still conventional ^{15}N CPMG experiments are limited to motions around 150 μs (ν_{CPMG} ~ 1 kHz) [135]. Taken together, since supra-τ_c motion can reside past this limit, $R_{1\rho}$ can be used in hopes of gaining access to the kinetics from this time-scale.

3.4. Off-Resonance $R_{1\rho}$ in Super-Cooled Conditions

Kinetics from the supra-τ_c range measured by off-resonance $R_{1\rho}$ was recently performed on the protein ubiquitin free in solution [115]. This study characterized a rapid microsecond process within the ground-state ensemble of ubiquitin whose rate of conformer interconversion has implications for its molecular recognition process [115,185,186]. At high temperatures, ubiquitin does not report on having an exchange contribution to $R_{1\rho}$ [70]. The authors hypothesized that if the motion escaped detection at higher temperatures then by lowering the temperature the lifetime of motion would increase making it accessible by off-resonance $R_{1\rho}$. Experiments were performed by super-cooling the sample to 265 K whereby significant RD was detected and a τ_{ex} of 120 μs was determined [115]. Following the temperature dependence of this motion, an Arrhenius extrapolation identified that the motion at physiological temperatures is between 1 and 19 μs. This motion has been attributed to the interconversion between distinct ubiquitin conformers and was corroborated with predicted Φ_{ex} values from the RDC derived ensembles [28,116], as well as measurements in solution using dielectric relaxation spectroscopy [115,187]. Although dielectric relaxation does not maintain atomic resolution like RD experiments, an Arrhenius extrapolation of the conformer interconversion lifetime is not required. Even with this milestone of measuring RD at super-cooled temperatures, only limited information with respect to the expansiveness of this motion could be attained because only a few sites within ubiquitin were detectable.

3.5. Exceeding the Limit with Cryogenically Cooled Probeheads

A prime limitation in RD experiments is the minimum accessible time-scale. Equation (44) has a Lorentzian form and therefore the smallest lifetime that can be observed is limited to the natural line width of a Lorentzian, which is controlled by ω_{eff} ($\tau_{ex} \approx 1/\omega_{eff}$). For the observation of exchange events, ω_{eff} depends on both ν_{RF} and Ω. Since these are both experimentally controlled parameters, they can be changed, but a compromise has to be made with respect to the tilt angle. A caveat emerges in which larger Ω values will cause the $R_{1\rho}$ value to be dominated by R_1 ($\cos^2(\theta)$ approaches 1), which in turn minimizes the contribution of R_{ex}. Thus, increases in ν_{RF}, instead of Ω, would provide a means of further extending $R_{1\rho}$ based RD techniques into the supra-τ_c range.

Recently, the previous limitations were exceeded through the use of hardware that is found in many NMR based laboratories, the cryogenically cooled probehead (cryo-probehead). A Bruker QCI S3 cryo-probehead was demonstrated to be capable of safely withstanding ν_{RF} values up to 6.4 kHz and represents an improvement by a factor of three from what was previously accepted [26]. This larger attainable spin-lock field strength permits a time resolution for motion up to 25 μs. On-resonance $R_{1\rho}$ experiments for ^{15}N nuclei within ubiquitin that had been previously shown to have dispersion were performed as validation for the use of large amplitude ν_{RF} [115,185]. Additional advantages also emerged when a cryo-probehead was used for RD measurements. Since a major aspect in relaxation experiments is to attain sufficient signal to noise that minimizes the errors in the obtained rates, measurement with a helium cooled NMR coil and pre-amplifier fulfills exactly this requirement via a noise reduction in those electronic components. Therefore, $R_{1\rho}$ rates could be monitored with increased precision. Given the increased precision in the measured rates, the errors in the extracted exchange parameters also decreased. More importantly, the implementation of on-resonance experiments removes any contribution from R_1 and tilt angle to the measured rate. Thus, any observed conformational exchange is solely modulated by ν_{RF}. The on-resonance RD measurement allows for a more complete sampling of the R_{ex} contribution. Furthermore, a ^{15}N site that undergoes smaller amplitude motion within the supra-τ_c range can be detected. The use of large amplitude spin-lock field strengths also purported more accurate intrinsic relaxation rates because exchange events up to 25 μs could be removed from $R_{2,eff}$ [26]. The application of more efficient quenching of conformational exchange has been recently demonstrated for the measurement of veracious intrinsic relaxation rates that supplement constant time CPMG type RD experiments [171]. An experiment was created (HEROINE) in which the same averaged coherence is monitored, but large amplitude ν_{RF} are employed permitting more accurate and precise kinetics to be extracted from CT-CPMG data even when motion is in the fast regime [188] ($(\tau_{ex}\,\omega)^{-1} > 3$) The use of large ν_{RF} may also be extended to nuclei with a larger gyromagnetic ratio (γ) as the achievable ν_{RF} scales with this value ($\nu_{RF} = \gamma B_{RF}/2\pi$) and even larger ν_{RF} could then potentially be applied [189–191]. Ultimately, large amplitude ν_{RF} based $R_{1\rho}$ appears to be a promising approach to the further quantification of kinetics from the supra-τ_c range.

3.6. Experimental Aspects for Kinetic Measurements in the Supra-τ_c Range

Experimental outlines for the execution of off/on-resonance $R_{1\rho}$ experiments for ^{15}N nuclei have been given in many reviews and texts [132,135,159,160,192], but details pertaining to super-cooled

and large amplitude ν_{RF} measurements will be discussed here. Initially demonstrated by Szyperski and coworkers, super-cooled relaxation measurements can be used to probe sub-τ_c events [193,194]. Under super-cooled conditions, the surface tension of the water increases resulting in a lower freezing point for a liquid solution. The NMR sample is initially centrifugated for a sufficient time in order to remove any potential nucleation points for ice formation. The samples can be placed into 1 mm NMR tubes, which are then filled with the liquid samples and subsequently flame sealed. Approximately ten to twelve 1 mm NMR tubes can be placed into a 5 mm tube, which is then inserted in the NMR magnet. Cooling to the desired temperature should be done in small increments and the sample given sufficient time in between temperature decrements for equilibration. As the temperature decreases, the line broadening of the NMR peaks is increased due to an increase in τ_c and/or due to slowing down the rates of conformational exchange processes. In order to enhance the sensitivity, $R_{1\rho}$ based RD can be performed by either querying the narrower doublet for ^{15}N nuclei [195,196] or by a conventional pulse sequence equipped with a TROSY [197,198] readout to maximize the longevity of the NMR signal. Additionally, TROSY is without decoupling during acquisition and therefore the overall heating can be reduced.

For the measurement of large amplitude ν_{RF}, the proper calibration of useable spin-lock field strengths must be ascertained. Continuous wave (CW) off-resonance decoupling experiments are a facile way to determine these amplitudes. CW-fields are applied off-resonance during the acquisition of a two-dimensional correlation experiment (e.g., [^{1}H, ^{15}N]-HSQC) that will cause some amount of partial decoupling. This partial decoupling translates to an effective scalar coupling value which can be correlated with respect to the Ω of a given resonance position [160,192]. A linear correlation between the scalar coupling values and Ω yields a line whose slope is ν_{RF} [26,160]. The collection of enough points during the acquisition period provides a way to determine the spin-lock amplitudes and lengths that can be safely applied on a given probehead. Of extreme importance is the utilization of recycle delays that are long enough to ensure a duty cycle that does not exceed 5% and that maintain the NMR coil temperature and preamp power reserve at a stable level. Heating due to the electric field component of a radio-frequency pulse can be differential between different experiments. Temperature compensation schemes should be implemented, which not only considers the length that ν_{RF} is applied, but also the amplitude of ν_{RF} in order to equalize the temperature between experiments [199]. The relative change in the temperature can be determined from $^{1}H^{N}$ temperature coefficients.

The acquisition of RD data can be conducted by varying ν_{RF} and/or Ω. With a given configuration, signal intensities are tracked by measuring their time dependence either by observing a full exponential decay or with two-point sampling schemes. Error estimation and application of different sampling techniques have been previously discussed [135,173,200]. Discerning possible dispersion profiles can be done by following particular selection criteria (i.e. minimum differences in relaxation rates) [147]. From here, the analysis of dispersion data is conducted by standard minimization protocols [132,135], in which the data are fit to models that are with and without conformational exchange contributions. Statistical tests, such as F-tests [201], can be applied in order to identify the better fitting model.

4. Conclusions and Outlook

The dynamic characterization of motions from the supra-τ_c range has been made possible by the careful dissemination of RDC data collected in unique alignment conditions [102,104,113]. The analysis of such information relies on model dependent (GAF; Section 2.4) [109–111] and model independent techniques (MFA, DIDC, SCRM and ORIUM; Section 2.3) [68,72,101,102,104,105]. Insight from such data has highlighted molecular motions related to molecular recognition for ubiquitin [28] and TAR-RNA [202], which were only realized with the inclusion of RDC data. RD is also emerging as an experimental tool to capture the kinetics from the supra-τ_c range [26,115]. Further methodological advancement will be required to try to completely sample this four orders of magnitude time window, however motion as fast as ~25 μs can be accessed with atomic resolution [26] based on variance of ^{15}N chemical shifts and even faster for nuclei with a larger gyromagnetic ratio. The harmony between experiment and computer simulation can also aid in accelerating studies of protein dynamics from supra-τ_c range. The RDC-derived ensembles [28,115,116] have shown that they faithfully include structural variances within the supra-τ_c range, and can also be used to have predictive power in identifying sites that may undergo conformational exchange that could be detectable by RD. Additionally, long MD trajectories and AMD type simulations have been able to identify supra-τ_c motion for the backbone of BPTI [20] and for example thrombin [120,121], respectively. A major goal for the future will be to see these experimental and computational techniques applied to an increased number of other biological macromolecules in order to enhance our understanding of the complex behavior displayed by biological macromolecules within the supra-τ_c window.

Acknowledgments

This paper is dedicated to Richard R. Ernst on the occasion of his 80th birthday. This work has been supported by the Max Planck Society and the EU (ERC grant agreement number 233227). We would like to acknowledge Mikael Akke and Nils Alexander Lakomek for helpful discussions. We would also like to acknowledge Helena Kovacs, Roberto Seydoux, Klemens Kessler, Detlef Moskau and Rainer Kümmerle at Bruker BioSpin AG for the helpful discussions pertaining to cryo-probehead technology.

Conflicts of Interest

The authors declare no conflict of interest.

References

1. Palmer III, A.G. NMR characterization of the dynamics of biomacromolecules. *Chem. Rev.* **2004**, *104*, 3623–3640.
2. Meier, B.H.; Ernst, R.R. Elucidation of Chemical-Exchange Networks by 2-Dimensional NMR-Spectroscopy — Heptamethylbenzenonium Ion. *J. Am. Chem. Soc.* **1979**, *101*, 6441–6442.
3. Wagner, G.; Bodenhausen, G.; Müller, N.; Rance, M.; Sørensen, O.W.; Ernst, R.R.; Wüthrich, K. Exchange of two-spin order in nuclear magnetic resonance: Separation of exchange and cross-relaxation processes. *J. Am. Chem. Soc.* **1985**, *107*, 6440–6446.

4. Chapman, B.E.; Stewart, I.M.; Bulliman, B.T.; Mendz, G.L.; Kuchel, P.W. ^{31}P Magnetization Transfer in the Phosphoglyceromutase-Enolase Coupled Enzyme-System. *Eur. Biophys. J.* **1988**, *16*, 187–191.
5. Kuchel, P.W.; Bulliman, B.T.; Chapman, B.E. Mutarotase equilibrium exchange kinetics studied by ^{13}C-NMR. *Biophys. Chem.* **1988**, *32*, 89–95.
6. Mendz, G.L.; Robinson, G.; Kuchel, P.W. Direct quantitative-analysis of enzyme-catalyzed reactions by two-dimensional nuclear-magnetic-resonance spectroscopy–Adenylate kinase and phosphoglyceromutase. *J. Am. Chem. Soc.* **1986**, *108*, 169–173.
7. Farrow, N.A.; Zhang, O.W.; Forman-Kay, J.D.; Kay, L.E. A Heteronuclear correlation experiment for simultaneous determination of 15n longitudinal decay and chemical-exchange rates of systems in slow equilibrium. *J. Biomol. NMR* **1994**, *4*, 727–734.
8. Wider, G.; Neri, D.; Wüthrich, W. Studies of slow conformational equilibria in macromolecules by exchange of heteronuclear longitudinal 2-spin-order in a 2D difference correlation experiment. *J. Biomol. NMR* **1991**, *1*, 93–98.
9. Haupt, C.; Patzschke, R.; Weininger, U.; Gröger, S.; Kovermann, M.; Balbach, J. Transient enzyme-substrate recognition monitored by real-time NMR. *J. Am. Chem. Soc.* **2011**, *133*, 11154–11162.
10. Zeeb, M.; Balbach, J. Protein folding studied by real-time NMR spectroscopy. *Methods* **2004**, *34*, 65–74.
11. Schanda, P.; Brutscher, B. Very fast two-dimensional NMR spectroscopy for real-time investigation of dynamic events in proteins on the time scale of seconds. *J. Am. Chem. Soc.* **2005**, *127*, 8014–8015.
12. Frydman, L.; Scherf, T.; Lupulescu, A. The acquisition of multidimensional NMR spectra within a single scan. *Proc. Nat. Acad. Sci. USA* **2002**, *99*, 15858–15862.
13. Rennella, E.; Cutuil, T.; Schanda, P.; Ayala, I.; Forge, V.; Brutscher, B. Real-time NMR characterization of structure and dynamics in a transiently populated protein folding intermediate. *J. Am. Chem. Soc.* **2012**, *134*, 8066–8069.
14. Bowen, S.; Hilty, C. Time-resolved dynamic nuclear polarization enhanced NMR spectroscopy. *Angew. Chem. Int. Edit.* **2008**, *47*, 5235–5237.
15. Harris, T.; Giraudeau, P.; Frydman, L. Kinetics from indirectly detected hyperpolarized NMR spectroscopy by using spatially selective coherence transfers. *Chem. Eur. J.* **2011**, *17*, 697–703.
16. Berjanskii, M.V.; Wishart, D.S. A simple method to predict protein flexibility using secondary chemical shifts. *J. Am. Chem. Soc.* **2005**, *127*, 14970–14971.
17. Li, D.W.; Brüschweiler, R. Certification of molecular dynamics trajectories with NMR chemical shifts. *J. Phys. Chem. Lett.* **2010**, *1*, 246–248.
18. Robustelli, P.; Stafford, K.A.; Palmer, A.G. Interpreting protein structural dynamics from NMR chemical shifts. *J. Am. Chem. Soc.* **2012**, *134*, 6365–6374.
19. Xue, Y.; Ward, J.M.; Yuwen, T.R.; Podkorytov, I.S.; Skrynnikov, N.R. Microsecond time-scale conformational exchange in proteins: Using long molecular dynamics trajectory to simulate NMR relaxation dispersion data. *J. Am. Chem. Soc.* **2012**, *134*, 2555–2562.

20. Shaw, D.E.; Maragakis, P.; Lindorff-Larsen, K.; Piana, S.; Dror, R.O.; Eastwood, M.P.; Bank, J.A.; Jumper, J.M.; Salmon, J.K.; Shan, Y.B.; Wriggers, W. Atomic-level characterization of the structural dynamics of proteins. *Science* **2010**, *330*, 341–346.
21. Reif, B.; Hennig, M.; Griesinger, C. Direct measurement of angles between bond vectors in high-resolution NMR. *Science* **1997**, *276*, 1230–1233.
22. Vögeli, B. Comprehensive description of NMR cross-correlated relaxation under anisotropic molecular tumbling and correlated local dynamics on all time scales. *J. Chem. Phys.* **2010**, *133*, 014501:1–014501:13.
23. Vugmeyster, L.; Pelupessy, P.; Vugmeister, B.E.; Abergel, D.; Bodenhausen, G. Cross-correlated relaxation in NMR of macromolecules in the presence of fast and slow internal dynamics. *C.R. Phys.* **2004**, *5*, 377–386.
24. Pelupessy, P.; Ravindranathan, S.; Bodenhausen, G. Correlated motions of successive amide N-H bonds in proteins. *J. Biomol. NMR* **2003**, *25*, 265–280.
25. Vögeli, B.; Yao, L.S. Correlated dynamics between protein hn and hc bonds observed by NMR cross relaxation. *J. Am. Chem. Soc.* **2009**, *131*, 3668–3678.
26. Ban, D.; Gossert, A.D.; Giller, K.; Becker, S.; Griesinger, C.; Lee, D. Exceeding the limit of dynamics studies on biomolecules using high spin-lock field strengths with a cryogenically cooled probehead. *J. Magn. Reson.* **2012**, *221*, 1–4.
27. Lakomek, N.A.; Carlomagno, T.; Becker, S.; Griesinger, C.; Meiler, J. A thorough dynamic interpretation of residual dipolar couplings in ubiquitin. *J. Biomol. NMR* **2006**, *34*, 101–115.
28. Lange, O.F.; Lakomek, N.A.; Farés, C.; Schröder, G.F.; Walter, K.F.; Becker, S.; Meiler, J.; Grubmüller, H.; Griesinger, C.; de Groot, B.L. Recognition dynamics up to microseconds revealed from an RDC-derived ubiquitin ensemble in solution. *Science* **2008**, *320*, 1471–1475.
29. Tjandra, N.; Bax, A. Direct measurement of distances and angles in biomolecules by NMR in a dilute liquid crystalline medium. *Science* **1997**, *278*, 1111–1114.
30. Tolman, J.R.; Flanagan, J.M.; Kennedy, M.A.; Prestegard, J.H. NMR evidence for slow collective motions in cyanometmyoglobin. *Nat. Struct. Mol. Biol.* **1997**, *4*, 292–297.
31. Saupe, A.; Englert, G. High-resolution nuclear magnetic resonance spectra of orientated molecules. *Phys. Rev. Lett.* **1963**, *11*, 462–464.
32. Saupe, A. Kernresonanzen in kristallinen flüssigkeiten und in kristallinflussigen lösungen. I. *Z. Naturforsch. A* **1964**, *A 19*, 161–171.
33. Saupe, A. Recent results in field of liquid crystals. *Angew. Chem. Int. Edit.* **1968**, *7*, 97–118.
34. Snyder, L.C. Analysis of nuclear magnetic resonance spectra of molecules in liquid-crystal solvents. *J. Chem. Phys.* **1965**, *43*, 4041–4050.
35. Gayathri, C.; Bothner-By, A.A.; van Zijl, P.C.M.; Maclean, C. Dipolar magnetic-field effects in NMR-spectra of liquids. *Chem. Phys. Lett.* **1982**, *87*, 192–196.
36. Lohman, J.A.B.; Maclean, C. Alignment Effects on High-Resolution NMR-spectra, Induced by the magnetic-field. *Chem. Phys.* **1978**, *35*, 269–274.
37. van Zijl, P.C.M.; Ruessink, B.H.; Bulthuis, J.; Maclean, C. NMR of partially aligned liquids–Magnetic-susceptibility anisotropies and dielectric-properties. *Acc. Chem. Res.* **1984**, *17*, 172–180.

38. Celebre, G.; Longeri, M.; Emsley, J.W. The Nature of the internal rotational barrier in benzyl-chloride - an interpretation of the dipolar coupling-constants obtained from the analysis of the proton NMR-spectra of samples dissolved in liquid-crystal solvents. *Mol. Phys.* **1988**, *64*, 715–723.
39. Celebre, G.; Longeri, M.; Emsley, J.W. An investigation by NMR-spectroscopy of the dependence on internal motion of the orientational ordering of ethoxybenzene and 4-fluoroethoxybenzene when dissolved in a nematic solvent. *Liq. Cryst.* **1989**, *6*, 689–700.
40. Counsell, C.J.R.; Emsley, J.W.; Luckhurst, G.R.; Sachdev, H.S. Orientational order in the 4-*n*-alkyloxy-4'-cyanobiphenyls–a comparison between experiment and theory. *Mol. Phys.* **1988**, *63*, 33–47.
41. Emsley, J.W.; Foord, E.K.; Gandy, P.J.F.; Turner, D.L.; Zimmermann, H. Assignment of the quadrupolar splittings in fully deuteriated alkyl chains of liquid-crystalline compounds–the case of 4-*n*-hexyloxy-4'-cyanobiphenyl. *Liq. Cryst.* **1994**, *17*, 303–309.
42. Emsley, J.W.; Heaton, N.J.; Kimmings, M.K.; Longeri, M. The conformation and orientational order of 1-ethoxy-4-chlorobenzene dissolved in a nematic liquid-crystal. *Mol. Phys.* **1987**, *61*, 433–442.
43. Emsley, J.W.; Luckhurst, G.R. The effect of internal motion on the orientational order parameters for liquid-crystalline systems. *Mol. Phys.* **1980**, *41*, 19–29.
44. Emsley, J.W.; Luckhurst, G.R.; Stockley, C.P. The deuterium and proton-(Deuterium) NMR-spectra of the partially deuteriated nematic liquid-crystal 4-*n*-pentyl-4'-cyanobiphenyl. *Mol. Phys.* **1981**, *44*, 565–580.
45. Rosen, M.E.; Rucker, S.P.; Schmidt, C.; Pines, A. 2-Dimensional proton NMR-studies of the conformations and orientations of *n*-alkanes in a liquid-crystal solvent. *J. Phys. Chem.* **1993**, *97*, 3858–3866.
46. Sinton, S.W.; Zax, D.B.; Murdoch, J.B.; Pines, A. Multiple-quantum NMR-study of molecular-structure and ordering in a liquid-crystal. *Mol. Phys.* **1984**, *53*, 333–362.
47. Tolman, J.R.; Flanagan, J.M.; Kennedy, M.A.; Prestegard, J.H. Nuclear magnetic dipole interactions in field-oriented proteins–information for structure determination in solution. *Proc. Nat. Acad. Sci. USA* **1995**, *92*, 9279–9283.
48. Kung, H.C.; Wang, K.Y.; Goljer, I.; Bolton, P.H. Magnetic alignment of duplex and quadruplex DNAs. *J. Magn. Reson. Ser. B* **1995**, *109*, 323–325.
49. Tjandra, N.; Grzesiek, S.; Bax, A. Magnetic field dependence of nitrogen-proton J splittings in N-15-enriched human ubiquitin resulting from relaxation interference and residual dipolar coupling. *J. Am. Chem. Soc.* **1996**, *118*, 6264–6272.
50. Clore, G.M.; Starich, M.R.; Gronenborn, A.M. Measurement of residual dipolar couplings of macromolecules aligned in the nematic phase of a colloidal suspension of rod-shaped viruses. *J. Am. Chem. Soc.* **1998**, *120*, 10571–10572.
51. Hansen, M.R.; Mueller, L.; Pardi, A. Tunable alignment of macromolecules by filamentous phage yields dipolar coupling interactions. *Nat. Struct. Mol. Biol.* **1998**, *5*, 1065–1074.
52. Hansen, M.R.; Rance, M.; Pardi, A. Observation of long-range H-1-H-1 distances in solution by dipolar coupling interactions. *J. Am. Chem. Soc.* **1998**, *120*, 11210–11211.

53. Barrientos, L.G.; Dolan, C.; Gronenborn, A.M. Characterization of surfactant liquid crystal phases suitable for molecular alignment and measurement of dipolar couplings. *J. Biomol. NMR* **2000**, *16*, 329–337.
54. Prosser, R.S.; Losonczi, J.A.; Shiyanovskaya, I.V. Use of a novel aqueous liquid crystalline medium for high-resolution NMR of macromolecules in solution. *J. Am. Chem. Soc.* **1998**, *120*, 11010–11011.
55. Rückert, M.; Otting, G. Alignment of biological macromolecules in novel nonionic liquid crystalline media for NMR experiments. *J. Am. Chem. Soc.* **2000**, *122*, 7793–7797.
56. Chou, J.J.; Gaemers, S.; Howder, B.; Louis, J.M.; Bax, A. A simple apparatus for generating stretched polyacrylamide gels, yielding uniform alignment of proteins and detergent micelles. *J. Biomol. NMR* **2001**, *21*, 377–382.
57. Sass, H.J.; Musco, G.; Stahl, S.J.; Wingfield, P.T.; Grzesiek, S. Solution NMR of proteins within polyacrylamide gels: Diffusional properties and residual alignment by mechanical stress or embedding of oriented purple membranes. *J. Biomol. NMR* **2000**, *18*, 303–309.
58. Tycko, R.; Blanco, F.J.; Ishii, Y. Alignment of biopolymers in strained gels: A new way to create detectable dipole-dipole couplings in high-resolution biomolecular NMR. *J. Am. Chem. Soc.* **2000**, *122*, 9340–9341.
59. Koenig, B.W.; Hu, J.S.; Ottiger, M.; Bose, S.; Hendler, R.W.; Bax, A. NMR measurement of dipolar couplings in proteins aligned by transient binding to purple membrane fragments. *J. Am. Chem. Soc.* **1999**, *121*, 1385–1386.
60. Sass, J.; Cordier, F.; Hoffmann, A.; Cousin, A.; Omichinski, J.G.; Lowen, H.; Grzesiek, S. Purple membrane induced alignment of biological macromolecules in the magnetic field. *J. Am. Chem. Soc.* **1999**, *121*, 2047–2055.
61. Bax, A.; Kontaxis, G.; Tjandra, N. Dipolar couplings in macromolecular structure determination. *Methods Enzymol.* **2001**, *339*, 127–174.
62. Chen, K.; Tjandra, N. The use of residual dipolar coupling in studying proteins by NMR. *Top. Curr. Chem.* **2012**, *326*, 47–67.
63. Tolman, J.R.; Ruan, K. NMR residual dipolar couplings as probes of biomolecular dynamics. *Chem. Rev.* **2006**, *106*, 1720–1736.
64. Bax, A.; Vuister, G.W.; Grzesiek, S.; Delaglio, F.; Wang, A.C.; Tschudin, R.; Zhu, G. Measurement of Homonuclear and Heteronuclear J-Couplings from Quantitative J-Correlation. *Methods Enzymol.* **1994**, *239*, 79–105.
65. Prestegard, J.H.; Al-Hashimi, H.M.; Tolman, J.R. NMR structures of biomolecules using field oriented media and residual dipolar couplings. *Quart. Rev. Biophys.* **2000**, *33*, 371–424.
66. Prestegard, J.H.; Mayer, K.L.; Valafar, H.; Benison, G.C. Determination of protein backbone structures from residual dipolar couplings. *Methods Enzymol.* **2005**, *394*, 175–209.
67. Losonczi, J.A.; Andrec, M.; Fischer, M.W.F.; Prestegard, J.H. Order matrix analysis of residual dipolar couplings using singular value decomposition. *J. Magn. Reson.* **1999**, *138*, 334–342.
68. Tolman, J.R. A novel approach to the retrieval of structural and dynamic information from residual dipolar couplings using several oriented media in biomolecular NMR spectroscopy. *J. Am. Chem. Soc.* **2002**, *124*, 12020–12030.

69. Zweckstetter, M. NMR: Prediction of molecular alignment from structure using the PALES software. *Nat. Protoc.* **2008**, *3*, 679–690.
70. Zweckstetter, M.; Bax, A. Prediction of sterically induced alignment in a dilute liquid crystalline phase: Aid to protein structure determination by NMR. *J. Am. Chem. Soc.* **2000**, *122*, 3791–3792.
71. Valafar, H.; Prestegard, J.H. REDCAT: A residual dipolar coupling analysis tool. *J. Magn. Reson.* **2004**, *167*, 228–241.
72. Meiler, J.; Prompers, J.J.; Peti, W.; Griesinger, C.; Brüschweiler, R. Model-free approach to the dynamic interpretation of residual dipolar couplings in globular proteins. *J. Am. Chem. Soc.* **2001**, *123*, 6098–6107.
73. Louhivuori, M.; Otten, R.; Lindorff-Larsen, K.; Annila, A. Conformational fluctuations affect protein alignment in dilute liquid crystal media. *J. Am. Chem. Soc.* **2006**, *128*, 4371–4376.
74. Salvatella, X.; Richter, B.; Vendruscolo, M. Influence of the fluctuations of the alignment tensor on the analysis of the structure and dynamics of proteins using residual dipolar couplings. *J. Biomol. NMR* **2008**, *40*, 71–81.
75. Bernadó, P.; Blanchard, L.; Timmins, P.; Marion, D.; Ruigrok, R.W.H.; Blackledge, M. A structural model for unfolded proteins from residual dipolar couplings and small-angle x-ray scattering. *Proc. Nat. Acad. Sci. USA* **2005**, *102*, 17002–17007.
76. Bertoncini, C.W.; Jung, Y.S.; Fernández, C.O.; Hoyer, W.; Griesinger, C.; Jovin, T.M.; Zweckstetter, M. Release of long-range tertiary interactions potentiates aggregation of natively unstructured alpha-synuclein. *Proc. Nat. Acad. Sci. USA* **2005**, *102*, 1430–1435.
77. Rodriguez-Castañeda, F.; Haberz, P.; Leonov, A.; Griesinger, C. Paramagnetic tagging of diamagnetic proteins for solution NMR. *Magn. Reson. Chem.* **2006**, *44*, S10-S16.
78. Bertini, I.; Del Bianco, C.; Gelis, I.; Katsaros, N.; Luchinat, C.; Parigi, G.; Peana, M.; Provenzani, A.; Zoroddu, M.A. Experimentally exploring the conformational space sampled by domain reorientation in calmodulin. *Proc. Nat. Acad. Sci. USA* **2004**, *101*, 6841–6846.
79. Zhang, Q.; Throolin, R.; Pitt, S.W.; Serganov, A.; Al-Hashimi, H.M. Probing motions between equivalent RNA domains using magnetic field induced residual dipolar couplings: Accounting for correlations between motions and alignment. *J. Am. Chem. Soc.* **2003**, *125*, 10530–10531.
80. Louhivuori, M.; Päätkönen, K.; Fredriksson, K.; Permi, P.; Lounila, J.; Annila, A. On the origin of residual dipolar couplings from denatured proteins. *J. Am. Chem. Soc.* **2003**, *125*, 15647–15650.
81. Shortle, D.; Ackerman, M.S. Persistence of native-like topology in a denatured protein in 8 M urea. *Science* **2001**, *293*, 487–489.
82. Ozenne, V.; Bauer, F.; Salmon, L.; Huang, J.R.; Jensen, M.R.; Segard, S.; Bernadó, P.; Charavay, C.; Blackledge, M. Flexible-meccano: a tool for the generation of explicit ensemble descriptions of intrinsically disordered proteins and their associated experimental observables. *Bioinformatics* **2012**, *28*, 1463–1470.
83. Jensen, M.R.; Houben, K.; Lescop, E.; Blanchard, L.; Ruigrok, R.W.H.; Blackledge, M. Quantitative conformational analysis of partially folded proteins from residual dipolar couplings: Application to the molecular recognition element of Sendai virus nucleoprotein. *J. Am. Chem. Soc.* **2008**, *130*, 8055–8061.

84. Nodet, G.; Salmon, L.; Ozenne, V.; Meier, S.; Jensen, M.R.; Blackledge, M. Quantitative description of backbone conformational sampling of unfolded proteins at amino acid resolution from NMR residual dipolar couplings. *J. Am. Chem. Soc.* **2009**, *131*, 17908–17918.
85. Skrynnikov, N.R.; Goto, N.K.; Yang, D.W.; Choy, W.Y.; Tolman, J.R.; Mueller, G.A.; Kay, L.E. Orienting domains in proteins using dipolar couplings measured by liquid-state NMR: Differences in solution and crystal forms of maltodextrin binding protein loaded with beta-cyclodextrin. *J. Mol. Biol.* **2000**, *295*, 1265–1273.
86. Koehler, J.; Meiler, J. Expanding the utility of NMR restraints with paramagnetic compounds: Background and practical aspects. *Prog. Nucl. Magn. Reson. Spectros.* **2011**, *59*, 360–389.
87. Xu, X.F.; Keizers, P.H.J.; Reinle, W.; Hannemann, F.; Bernhardt, R.; Ubbink, M. Intermolecular dynamics studied by paramagnetic tagging. *J. Biomol. NMR* **2009**, *43*, 247–254.
88. Xu, X.F.; Reinle, W.G.; Hannemann, F.; Konarev, P.V.; Svergun, D.I.; Bernhardt, R.; Ubbink, M. Dynamics in a pure encounter complex of two proteins studied by solution scattering and paramagnetic NMR spectroscopy. *J. Am. Chem. Soc.* **2008**, *130*, 6395–6403.
89. Barbieri, R.; Bertini, I.; Lee, Y.M.; Luchinat, C.; Velders, A.H. Structure-independent cross-validation between residual dipolar couplings originating from internal and external orienting media. *J. Biomol. NMR* **2002**, *22*, 365–368.
90. Bertini, I.; Gupta, Y.K.; Luchinat, C.; Parigi, G.; Peana, M.; Sgheri, L.; Yuan, J. Paramagnetism-based NMR restraints provide maximum allowed probabilities for the different conformations of partially independent protein domains. *J. Am. Chem. Soc.* **2007**, *129*, 12786–12794.
91. Pintacuda, G.; Keniry, M.A.; Huber, T.; Park, A.Y.; Dixon, N.E.; Otting, G. Fast structure-based assignment of ^{15}N HSQC spectra of selectively ^{15}N-labeled paramagnetic proteins. *J. Am. Chem. Soc.* **2004**, *126*, 2963–2970.
92. Otting, G. Protein NMR using paramagnetic ions. *Annu. Rev. Biophys.* **2010**, *39*, 387–405.
93. Gaponenko, V.; Altieri, A.S.; Li, J.; Byrd, R.A. Breaking symmetry in the structure determination of (large) symmetric protein dimers. *J. Biomol. NMR* **2002**, *24*, 143–148.
94. Gaponenko, V.; Sarma, S.P.; Altieri, A.S.; Horita, D.A.; Li, J.; Byrd, R.A. Improving the accuracy of NMR structures of large proteins using pseudocontact shifts as long-range restraints. *J. Biomol. NMR* **2004**, *28*, 205–212.
95. Wöhnert, J.; Franz, K.J.; Nitz, M.; Imperiali, B.; Schwalbe, H. Protein alignment by a coexpressed lanthanide-binding tag for the measurement of residual dipolar couplings. *J. Am. Chem. Soc.* **2003**, *125*, 13338–13339.
96. Barthelmes, K.; Reynolds, A.M.; Peisach, E.; Jonker, H.R.A.; DeNunzio, N.J.; Allen, K.N.; Imperiali, B.; Schwalbe, H. Engineering Encodable Lanthanide-Binding Tags into Loop Regions of Proteins. *J. Am. Chem. Soc.* **2011**, *133*, 808–819.
97. Zhang, Q.; Sun, X.Y.; Watt, E.D.; Al-Hashimi, H.M. Resolving the motional modes that code for RNA adaptation. *Science* **2006**, *311*, 653–656.
98. Zhang, Q.; Stelzer, A.C.; Fisher, C.K.; Al-Hashimi, H.M. Visualizing spatially correlated dynamics that directs RNA conformational transitions. *Nature* **2007**, *450*, 1263–1267.
99. Hus, J.C.; Brüschweiler, R. Principal component method for assessing structural heterogeneity across multiple alignment media. *J. Biomol. NMR* **2002**, *24*, 123–132.

100. Hus, J.C.; Peti, W.; Griesinger, C.; Brüschweiler, R. Self-consistency analysis of dipolar couplings in multiple alignments of ubiquitin. *J. Am. Chem. Soc.* **2003**, *125*, 5596–5597.
101. Peti, W.; Meiler, J.; Brüschweiler, R.; Griesinger, C. Model-free analysis of protein backbone motion from residual dipolar couplings. *J. Am. Chem. Soc.* **2002**, *124*, 5822–5833.
102. Lakomek, N.A.; Walter, K.F.; Farès, C.; Lange, O.F.; de Groot, B.L.; Grubmüller, H.; Brüschweiler, R.; Munk, A.; Becker, S.; Meiler, J.; *et al.* Self-consistent residual dipolar coupling based model-free analysis for the robust determination of nanosecond to microsecond protein dynamics. *J. Biomol. NMR* **2008**, *41*, 139–155.
103. Meirovitch, E.; Lee, D.; Walter, K.F.; Griesinger, C. Standard tensorial analysis of local ordering in proteins from residual dipolar couplings. *J. Phys. Chem. B* **2012**, *116*, 6106–6117.
104. Yao, L.; Vögeli, B.; Torchia, D.A.; Bax, A. Simultaneous NMR study of protein structure and dynamics using conservative mutagenesis. *J. Phys. Chem. B* **2008**, *112*, 6045–6056.
105. Sabo, T.M.; Smith, C.A.; Ban, D.; Mazur, A.; Lee, D.; Griesinger, C. ORIUM: Optimized RDC-based iterative and unified model-free analysis. *J. Biomol. NMR* **2013**, in press.
106. Bremi, T.; Brüschweiler, R. Locally anisotropic internal polypeptide backbone dynamics by NMR relaxation. *J. Am. Chem. Soc.* **1997**, *119*, 6672–6673.
107. Brüschweiler, R.; Wright, P.E. NMR order parameters of biomolecules—A new analytical representation and application to the gaussian axial fluctuation model. *J. Am. Chem. Soc.* **1994**, *116*, 8426–8427.
108. Lienin, S.F.; Bremi, T.; Brutscher, B.; Brüschweiler, R.; Ernst, R.R. Anisotropic intramolecular backbone dynamics of ubiquitin characterized by NMR relaxation and MD computer simulation. *J. Am. Chem. Soc.* **1998**, *120*, 9870–9879.
109. Bernadó, P.; Blackledge, M. Local dynamic amplitudes on the protein backbone from dipolar couplings: Toward the elucidation of slower motions in biomolecules. *J. Am. Chem. Soc.* **2004**, *126*, 7760–7761.
110. Bernadó, P.; Blackledge, M. Anisotropic small amplitude peptide plane dynamics in proteins from residual dipolar couplings. *J. Am. Chem. Soc.* **2004**, *126*, 4907–4920.
111. Bouvignies, G.; Bernadó, P.; Meier, S.; Cho, K.; Grzesiek, S.; Brüschweiler, R.; Blackledge, M. Identification of slow correlated motions in proteins using residual dipolar and hydrogen-bond scalar couplings. *Proc. Nat. Acad. Sci. USA* **2005**, *102*, 13885–13890.
112. Salmon, L.; Bouvignies, G.; Markwick, P.; Lakomek, N.; Showalter, S.; Li, D.W.; Walter, K.; Griesinger, C.; Brüschweiler, R.; Blackledge, M. Protein conformational flexibility from structure-free analysis of nmr dipolar couplings: Quantitative and absolute determination of backbone motion in ubiquitin. *Angew. Chem. Int. Edit.* **2009**, *48*, 4154–4157.
113. Salmon, L.; Pierce, L.; Grimm, A.; Roldan, J.L.O.; Mollica, L.; Jensen, M.R.; van Nuland, N.; Markwick, P.R.L.; McCammon, J.A.; Blackledge, M. Multi-timescale conformational dynamics of the sh3 domain of cd2-associated protein using NMR spectroscopy and accelerated molecular dynamics. *Angew. Chem. Int. Edit.* **2012**, *51*, 6103–6106.
114. Farès, C.; Lakomek, N.A.; Walter, K.F.A.; Frank, B.T.C.; Meiler, J.; Becker, S.; Griesinger, C. Accessing ns-µs side chain dynamics in ubiquitin with methyl RDCs. *J. Biomol. NMR* **2009**, *45*, 23–44.

115. Ban, D.; Funk, M.; Gulich, R.; Egger, D.; Sabo, T.M.; Walter, K.F.; Fenwick, R.B.; Giller, K.; Pichierri, F.; de Groot, B.L.; *et al.* Kinetics of conformational sampling in ubiquitin. *Angew. Chem. Int. Ed. Engl.* **2011**, *50*, 11437–11440.
116. Fenwick, R.B.; Esteban-Mart ń, S.; Richter, B.; Lee, D.; Walter, K.F.; Milovanovic, D.; Becker, S.; Lakomek, N.A.; Griesinger, C.; Salvatella, X. Weak long-range correlated motions in a surface patch of ubiquitin involved in molecular recognition. *J. Am. Chem. Soc.* **2011**, *133*, 10336–10339.
117. Hamelberg, D.; Mongan, J.; McCammon, J.A. Accelerated molecular dynamics: A promising and efficient simulation method for biomolecules. *J. Chem. Phys.* **2004**, *120*, 11919–11929.
118. Markwick, P.R.L.; Bouvignies, G.; Blackledge, M. Exploring multiple timescale motions in protein GB3 using accelerated molecular dynamics and NMR spectroscopy. *J. Am. Chem. Soc.* **2007**, *129*, 4724–4730.
119. Markwick, P.R.L.; Bouvignies, G.; Salmon, L.; McCammon, J.A.; Nilges, M.; Blackledge, M. Toward a unified representation of protein structural dynamics in solution. *J. Am. Chem. Soc.* **2009**, *131*, 16968–16975.
120. Fuglestad, B.; Gasper, P.M.; Tonelli, M.; McCammon, J.A.; Markwick, P.R.L.; Komives, E.A. The Dynamic Structure of Thrombin in Solution. *Biophys. J.* **2012**, *103*, 79–88.
121. Gasper, P.M.; Fuglestad, B.; Komives, E.A.; Markwick, P.R.L.; McCammon, J.A. Allosteric networks in thrombin distinguish procoagulant *vs.* anticoagulant activities. *Proc. Nat. Acad. Sci. USA* **2012**, *109*, 21216–21222.
122. Cervantes, C.F.; Markwick, P.R.L.; Sue, S.C.; McCammon, J.A.; Dyson, H.J.; Komives, E.A. Functional dynamics of the folded ankyrin repeats of iκbα revealed by nuclear magnetic resonance. *Biochemistry* **2009**, *48*, 8023–8031.
123. Farrow, N.A.; Muhandiram, R.; Singer, A.U.; Pascal, S.M.; Kay, C.M.; Gish, G.; Shoelson, S.E.; Pawson, T.; Forman-Kay, J.D.; Kay, L.E. Backbone dynamics of a free and phosphopeptide-complexed Src homology 2 domain studied by ^{15}N NMR relaxation. *Biochemistry* **1994**, *33*, 5984–6003.
124. Kay, L.E.; Torchia, D.A.; Bax, A. Backbone dynamics of proteins as studied by ^{15}N inverse detected heteronuclear NMR spectroscopy: Application to staphylococcal nuclease. *Biochemistry* **1989**, *28*, 8972–8979.
125. Cordier, F.; Brutscher, B.; Marion, D. Measurement of ^{13}Cα-^{13}CO cross-relaxation rates in ^{15}N-/^{13}C -labelled proteins. *J. Biomol. NMR* **1996**, *7*, 163–168.
126. Daragan, V.A.; Mayo, K.H. Motional model analyses of protein and peptide dynamics using ^{13}C and ^{15}N-NMR relaxation. *Prog. Nucl. Magn. Reson. Spectrosc.* **1997**, *31*, 63–105.
127. Muhandiram, D.R.; Yamazaki, T.; Sykes, B.D.; Kay, L.E. Measurement of ^{2}H T_1 and $T_{1\rho}$ relaxation times in uniformly ^{13}C-labeled and fractionally ^{2}H-labeled proteins in solution. *J. Am. Chem. Soc.* **1995**, *117*, 11536–11544.
128. Palmer III, A.G.; Rance, M.; Wright, P.E. Intramolecular motions of a zinc finger DNA-binding domain from XFIN characterized by proton-detected natural abundance ^{13}C heteronuclear NMR spectroscopy. *J. Am. Chem. Soc.* **1991**, *113*, 4371–4380.

129. Yamazaki, T.; Muhandiram, R.; Kay, L.E. NMR experiments for the measurement of carbon relaxation properties in highly enriched, uniformly ^{13}C, ^{15}N-labeled proteins: Application to ^{13}Cα carbons. *J. Am. Chem. Soc.* **1994**, *116*, 8266–7278.
130. Zeng, L.; Fischer, M.W.F.; Zuiderweg, E.R.P. Study of protein dynamics in solution by measurement of ^{13}Cα-^{13}CO NOE and ^{13}CO longitudinal relaxation. *J. Biomol. NMR* **1996**, *7*, 157–162.
131. Cavanagh, J.; Fairbrother, W.J.; Palmer III, A.G.; Rance, M.; Skelton, N.J. *Principles and Practice: Protein NMR Spectroscopy*, 2nd ed.; Elsevier: London, United Kingdom, 2007.
132. Korzhnev, D.M.; Billeter, M.; Arseniev, A.S.; Orekhov, V.Y. NMR studies of Brownian tumbling and internal motions in proteins. *Prog. Nucl. Magn. Reson. Spectros.* **2001**, *38*, 197–266.
133. Lüginbuhl, P.; Wüthrich, K. Semi-classical nuclear spin relaxation theory revisted for use with biological macromolecules. *Prog. Nucl. Magn. Reson. Spectros.* **2002**, *40*, 199–247.
134. Palmer III, A.G. NMR probes of molecular dynamics: Overview and comparison with other techniques. *Annu. Rev. Biophys. Biomol. Struct.* **2001**, *30*, 129–155.
135. Ishima, R. Recent developments in ^{15}N NMR relaxation studies that probe protein backbone dynamics. *Top. Curr. Chem.* **2012**, *326*, 99–122.
136. Lipari, G.; Szabo, A. Model-free approach to the interpretation of nuclear magnetic resonance relaxtion in macromolecules. 1. Theory and range of validity. *J. Am. Chem. Soc.* **1982**, *104*, 4546–4559.
137. Lipari, G.; Szabo, A. Model-Free approach to the interpretation of nuclear magnetic-resonance relaxation in macromolecules. 2. Analysis of experimental results. *J. Am. Chem. Soc.* **1982**, *104*, 4559–4570.
138. Yang, D.; Kay, L.E. Contributions to conformational entropy arising from bond vector fluctuations measured from NMR-derived order parameters: application to protein folding. *J. Mol. Biol.* **1996**, *263*, 369–382.
139. Akke, M.; Brüschweiler, R.; Palmer, A.G., 3rd NMR order parameters and free energy: an analytical approach and its application to cooperative Ca^{2+} binding by calbindin D9k. *J. Am. Chem. Soc.* **1993**, *115*, 9832–9833.
140. Lee, A.L.; Kinnear, S.A.; Wand, A.J. Redistribution and loss of side chain entropy upon formation of a calmodulin-peptide complex. *Nat. Struct. Biol.* **2000**, *7*, 72–77.
141. Sabo, T.M.; Bakhtiari, D.; Walter, K.F.A.; McFeeters, R.L.; Giller, K.; Becker, S.; Griesinger, C.; Lee, D. Thermal coefficients of the methyl groups within ubiquitin. *Protein Sci.* **2012**, *21*, 562–570.
142. Clore, G.M.; Szabo, A.; Bax, A.; Kay, L.E.; Driscoll, P.C.; Gronenborn, A.M. Deviations from the simple two-paramter model-free approach to the interpretation of nitrogen-15 nuclear magnetic relaxation of proteins. *J. Am. Chem. Soc.* **1990**, *112*, 4989–4991.
143. Tjandra, N.; Feller, S.E.; Pastor, R.W.; Bax, A. Rotational diffusion anisotropy of human ubiquitin from ^{15}N NMR relaxation. *J. Am. Chem. Soc.* **1995**, *117*, 12562–12566.
144. Baber, J.L.; Szabo, A.; Tjandra, N. Analysis of slow interdomain motion of macromolecules using NMR relaxation data. *J. Am. Chem. Soc.* **2001**, *123*, 3953–3959.
145. Brüschweiler, R.; Liao, X.; Wright, P.E. Long-range motional restrictions in a multidomain zinc-finger protein from anisotropic tumbling. *Science* **1995**, *268*, 886–889.

146. Jackson, S.E. How do small single-domain proteins fold? *Fold. Des.* **1998**, *3*, R81–R91.
147. Korzhnev, D.M.; Salvatella, X.; Vendruscolo, M.; Di Nardo, A.A.; Davidson, A.R.; Dobson, C.M.; Kay, L.E. Low-populated folding intermediates of Fyn SH3 characterized by relaxation dispersion NMR. *Nature* **2004**, *430*, 586–590.
148. Kubelka, J.; Hofrichter, J.; Eaton, W.A. The protein folding 'speed limit'. *Curr. Opin. Struct. Biol.* **2004**, *14*, 76–88.
149. Neira, J.L. NMR as a tool to identify and characterize protein folding intermediates. *Arch. Biochem. Biophys.* **2013**, *531*, 90–99.
150. Bhabha, G.; Lee, J.; Ekiert, D.C.; Gam, J.; Wilson, I.A.; Dyson, H.J.; Benkovic, S.J.; Wright, P.E. A dynamic knockout reveals that conformational fluctuations influence the chemical step of enzyme catalysis. *Science* **2011**, *332*, 234–238.
151. Boehr, D.D.; McElheny, D.; Dyson, H.J.; Wright, P.E. The dynamic energy landscape of dihydrofolate reductase catalysis. *Science* **2006**, *313*, 1638–1642.
152. Eisenmesser, E.Z.; Millet, O.; Labeikovsky, W.; Korzhnev, D.M.; Wolf-Watz, M.; Bosco, D.A.; Skalicky, J.J.; Kay, L.E.; Kern, D. Intrinsic dynamics of an enzyme underlies catalysis. *Nature* **2005**, *438*, 117–121.
153. Boehr, D.D.; Dyson, H.J.; Wright, P.E. An NMR perspective on enzyme catalysis. *Chem. Rev.* **2006**, *106*, 3055–3079.
154. Wang, L.; Pang, Y.; Holder, T.; Brender, J.R.; Kurochkin, A.V.; Zuiderweg, E.R.P. Functional dynamics in the active site of the ribonuclease binase. *Proc. Nat. Acad. Sci. USA* **2001**, *98*, 7684–7689.
155. Janin, J. The kinetics of protein-protein recognition. *Protein. Struct. Funct. Genet.* **1997**, *28*, 153–161.
156. McCammon, J.A. Theory of biomolecular recognition. *Curr. Opin. Struct. Biol.* **1998**, *8*, 245–249.
157. Sugase, K.; Dyson, H.J.; Wright, P.E. Mechanism of coupled folding and binding of an intrinsically disordered protein. *Nature* **2007**, *447*, 1021–1025.
158. Neudecker, P.; Lundström, P.; Kay, L.E. Relaxation dispersion NMR spectroscopy as a tool for detailed studies of protein folding. *Biophys. J.* **2009**, *96*, 2045–2054.
159. Palmer III, A.G.; Kroenke, C.D.; Loria, J.P. Nuclear magnetic resonance methods for quantifying microsecond-to-millisecond motions in biological macromolecules. *Methods Enzymol.* **2001**, *339*, 204–238.
160. Palmer III, A.G.; Massi, F. Characterization of the dynamics of biomacromolecules using rotating-frame spin relaxation NMR spectroscopy. *Chem. Rev.* **2006**, *106*, 1700–1719.
161. Luz, Z.; Meiboom, S. Nuclear magnetic resonance study of the protolysis of trimethylammonium ion in aqueous solution-order of the reaction with respect to solvent. *J. Chem. Phys.* **1963**, *39*, 366–370.
162. Wennerström, H. Nuclear magnetic relaxation induced by chemical exchange. *Mol. Phys.* **1972**, *24*, 69–80.
163. Millet, O.; Loria, J.P.; Kroenke, C.D.; Pons, M.; Palmer, A.G., 3rd. The static magnetic field dependence of chemical exchange linebroadening defines the NMR chemical shift time scale. *J. Am. Chem. Soc.* **2000**, *122*, 2867–2877.

164. Deverell, C.; Morgan, R.E.; Strange, J.H. Studies of chemical exchange by nuclear magnetic relaxation in the rotating frame. *Mol. Phys.* **1970**, *18*, 553–559.
165. Carr, H.Y.; Purcell, E.M. Effects of diffusion on free precession in nuclear magnetic resonance experiments. *Phys. Rev.* **1954**, *54*, 630–638.
166. Meiboom, S.; Gill, S. Modified spin-echo method for measuring nuclear relaxation times. *Rev. Sci. Instrum.* **1958**, *29*, 688–691.
167. Korzhnev, D.M.; Religa, T.L.; Banachewicz, W.; Fersht, A.R.; Kay, L.E. A transient and low-populated protein-folding intermediate at atomic resolution. *Science* **2010**, *329*, 1312–1316.
168. Mangia, S.; Traaseth, N.J.; Veglia, G.; Garwood, M.; Michaeli, S. Probing slow protein dynamics by adiabatic $R_{1\rho}$ and $R_{2\rho}$ NMR experiments. *J. Am. Chem. Soc.* **2010**, *132*, 9979–9981.
169. Traaseth, N.J.; Chao, F.; Masterson, L.R.; Mangia, S.; Garwood, M.; Michaeli, S.; Seelig, B.; Veglia, G. Heteronuclear adiabatic relaxation dispersion (HARD) for quantitative analysis of conformational dynamics in proteins. *J. Magn. Reson.* **2012**, *219*, 75–82.
170. Davis, D.G.; Perlman, M.E.; London, R.E. Direct measurements of the dissociation-rate constant for inhibitor-enzyme complexes via the $T_{1\rho}$ and T_2 (CPMG) methods. *J. Magn. Reson.* **1994**, *104*, 266–275.
171. Loria, J.P.; Rance, M.; Palmer III, A.G. A relaxation-compensated carr-purcell-meiboom-gill sequence for characterizing chemical exchange by nmr spectroscopy. *J. Am. Chem. Soc.* **1999**, *121*, 2331–2332.
172. Mulder, F.A.A.; Skrynnikov, N.R.; Hon, B.; Dahlquist, F.W.; Kay, L.E. Measurement of slow (micro- to millisecond) time scale dynamics in protein side chains by ^{15}N relaxation dispersion NMR spectroscopy: Application to Asn and Gln residues in a cavity mutant of T4 lysozyme. *J. Am. Chem. Soc.* **2001**, *123*, 967–975.
173. Skrynnikov, N.R.; Mulder, F.A.; Hon, B.; Dahlquist, F.W.; Kay, L.E. Probing slow time scale dynamics at methyl-containing side chains in proteins by relaxation dispersion NMR measurements: application to methionine residues in a cavity mutant of T4 lysozyme. *J. Am. Chem. Soc.* **2001**, *123*, 4556–4566.
174. Tollinger, M.; Skrynnikov, N.R.; Mulder, F.A.; Forman-Kay, J.D.; Kay, L.E. Slow dynamics in folded and unfolded states of an SH3 domain. *J. Am. Chem. Soc.* **2001**, *123*, 11341–11352.
175. Akke, M.; Liu, J.; Cavanagh, J.; Erickson, H.P.; Palmer III, A.G. Pervasive conformational fluctuations on microsecond time scales in a fibronectin type III domain. *Nat. Struct. Biol.* **1998**, *5*, 55–59.
176. Akke, M.; Palmer III, A.G. Monitoring macromolecular motions on microsecond to Milliesecond time scales by $R_{1\rho}$-R_1 constant relaxation time NMR spectrosocpy. *J. Am. Chem. Soc.* **1996**, *118*, 911–912.
177. Vugmeyster, L.; Kroenke, C.D.; Picart, F.; Palmer III, A.G.; Raleigh, P. ^{15}N R_{1r} measurements allow the determination of ultrafast protein folding rates. *J. Am. Chem. Soc.* **2000**, *122*, 5387–5388.
178. Dethoff, E.A.; Petzold, K.; Chugh, J.; Casiano-Negroni, A.; Al-Hashimi, H.M. Visualizing transient low-populated structures of RNA. *Nature* **2012**, *491*, 724–728.
179. Nikolova, E.N.; Kim, E.; Wise, A.A.; O'Brien, P.J.; Andricioaei, I.; Al-Hashimi, H.M. Transient hoogsteen base pairs in canonical duplex DNA. *Nature* **2011**, *470*, 498–502.

180. Ishima, R.; Torchia, D.A. Estimating the time scale of chemical exchange of proteins from measurements of transverse relaxation rates in solution. *J. Biomol. NMR* **1999**, *14*, 369–372.
181. Carver, J.P.; Richards, R.E. A general two-site solution for the chemical exchange produced dependence of T_2 upon the Carr-Purcell pulse separation. *J. Magn. Reson.* **1972**, *6*, 89–105.
182. Korzhnev, D.M.; Orekhov, V.Y.; Dahlquist, F.W.; Kay, L.E. Off-resonance $R_{1\rho}$ relaxation outside of the fast exchange limit: An experimental study of a cavity mutant of T4 lysozyme. *J. Biomol. NMR* **2003**, *26*, 39–48.
183. Korzhnev, D.M.; Orekhov, V.Y.; Kay, L.E. Off-resonance $R_{1\rho}$ NMR studies of exchange dynamics in proteins with low spin-lock fields: an application to a Fyn SH3 domain. *J. Am. Chem. Soc.* **2005**, *127*, 713–721.
184. Trott, O.; Palmer, A.G., 3rd. $R_{1\rho}$ relaxation outside of the fast-exchange limit. *J. Magn. Reson.* **2002**, *154*, 157–160.
185. Massi, F.; Grey, M.J.; Palmer, A.G., 3rd Microsecond timescale backbone conformational dynamics in ubiquitin studied with NMR $R_{1\rho}$ relaxation experiments. *Protein Sci.* **2005**, *14*, 735–742.
186. Salvi, N.; Ulzega, S.; Ferrage, F.; Bodenhausen, G. Timescales of slow motions in ubiquitin explored by heteronuclear double resonance. *J. Am. Chem. Soc.* **2012**, *134*, 2481–2484.
187. Wolf, M.; Gulich, R.; Lunkenheimer, P.; Loidl, A. Relaxation dynamics of a protein solution investigated by dielectric spectroscopy. *Biochim. Biophys. Acta* **2012**, *1824*, 723–730.
188. Ban, D.; Mazur, A.; Carneiro, M.G.; Sabo, T.M.; Giller, K.; Koharudin, L.M.I.; Becker, S.; Gronenborn, A.M.; Griesinger, C.; Lee, D. Enhanced accuracy of kinetic information from CT-CMPG experiments by transverse rotating-frame spectroscopy. *J. Biomol. NMR* **2013**, *57*, 73–82.
189. Ishima, R.; Wingfield, P.T.; Stahl, S.J.; Kaufman, J.D.; Torchia, D.A. Using amide ^{1}H and ^{15}N transverse relaxation to detect millisecond time-scale motions in perdeuterated proteins: application to HIV-1 protease. *J. Am. Chem. Soc.* **1998**, *120*, 10534–10542.
190. Ishima, R.; Torchia, D.A. Extending the range of amide proton relaxation dispersion experiments in proteins using a constant-time relaxation-compensated CPMG approach. *J. Biomol. NMR* **2003**, *25*, 243–248.
191. Eichmüller, C.; Skrynnikov, N.R. A new amide proton $R_{1\rho}$ experiment permits accurate characterization of microsecond time-scale conformational exchange. *J. Biomol. NMR* **2005**, *32*, 281–293.
192. Desvaux, H.; Berthault, P. Study of dynamic processes in liquids using off-resonance rf irradiation. *Prog. Nucl. Magn. Reson. Spectros.* **1999**, *35*, 295–340.
193. Mills, J.L.; Szyperski, T. Protein dynamics in supercooled water: the search for slow motional modes. *J. Biomol. NMR* **2002**, *23*, 63–67.
194. Skalicky, J.J.; Sukumaran, D.K.; Mills, J.L.; Szyperski, T. Toward structural biology in supercooled water. *J. Am. Chem. Soc.* **2000**, *122*, 3230–3231.
195. Igumenova, T.I.; Palmer, A.G., III. Off-Resonance TROSY-selected $R_{1\rho}$ experiment with improved sensitivity for medium- and high-molecular wegith proteins. *J. Am. Chem. Soc.* **2006**, *128*, 8110–8111.
196. Kempf, J.G.; Jung, J.; Sampson, N.S.; Loria, J.P. Off-resonance TROSY ($R_{1\rho}$-R_1) for quantitation of fast exchange processes in large proteins. *J. Am. Chem. Soc.* **2003**, *125*, 12064–12065.

197. Pervushin, K.; Riek, R.; Wider, G.; Wüthrich, K. Attenuated T_2 relaxation by mutual cancellation of dipole-dipole coupling and chemical shift anisotropy indicates an avenue to NMR structures of very large biological macromolecules in solution. *Proc. Nat. Acad. Sci. USA* **1997**, *94*, 12366–12371.
198. Nietlispach, D. Suppression of anti-TROSY lines in a sensitivity enhanced gradient selection TROSY scheme. *J. Biomol. NMR* **2005**, *31*, 161–166.
199. Wang, A.C.; Bax, A. Minimizing the effects of radio-frequency heating in multidimensional NMR experiments. *J. Biomol. NMR* **1993**, *3*, 715–720.
200. Jones, J.A.; Hodgkinson, P.; Barker, A.L.; Hore, P.J. Optimal sampling strategies for the measurement of spin-spin relaxation times. *J. Magn. Reson.* **1996**, *113*, 25–34.
201. Burnham, K.P.; Anderson, D.R. *Model Selection and Multi-Model Inference*; Springer: New York, NY, USA, 2002.
202. Al-Hashimi, H.M.; Gosser, Y.; Gorin, A.; Hu, W.D.; Majumdar, A.; Patel, D.J. Concerted motions in HIV-1 TAR RNA may allow access to bound state conformations: RNA dynamics from NMR residual dipolar couplings. *J. Mol. Biol.* **2002**, *315*, 95–102.

© 2013 by the authors; licensee MDPI, Basel, Switzerland. This article is an open access article distributed under the terms and conditions of the Creative Commons Attribution license (http://creativecommons.org/licenses/by/3.0/).